The scalar feed

Eindhoven University of Technology

Eindhoven The Netherlands

Department of Electrical Engineering

THE SCALAR FEED

by

J.K.M.Jansen, M.E.J.Jeuken, and C.W.Lambrechtse.

T.H.Report 70-E-12

20th November, 1969.

Contents

List of principal symbols

d = depth of a groove

b = width of a groove

t = thickness of dam

Θ_o = flare angle

r' = radius of the spherical aperture surface

r_1 = radius of boundary I of a spherical groove

r_2 = radius of boundary III of a spherical groove

ω = angular frequency

μ_o = permeability of free space

ε_o = permittivity of free space

$\underline{E}(\underline{r})$ = electric field

$\underline{H}(\underline{r})$ = magnetic field

m,n,ν = mode order numbers

k = propagation constant of plane waves in free space

a_n, b_n, c_{nm}, d_{nm}, e_m, f_m, A_1, A_2 = field amplitude coefficients

$F_r(r,\theta,\phi)$ = generating function of TE modes

$A_r(r,\theta,\phi)$ = generating function of TM modes

$j_n(kr)$ = spherical Bessel function of first kind and order n

$y_n(kr)$ = spherical Bessel function of the second kind and order n

$P_n^m(\cos\theta)$ = associated Legendre function of the first kind, of order m and degree n

$Q_n^m(\cos\theta)$ = associeted Legendre function of the second kind, of order m and degree n

θ_2 = angle which determines the boundary II of a spherical groove

l = integer

s = depth of a spherical groove measured along the boundary I

Z_o = impedance of plane waves in free space

λ = wavelength in free space

$H_\nu^{(2)}(kr')$ = spherical Hankelfunction of the second kind and order ν

$\xi_\nu(kr')$ = $\frac{1}{jk} \frac{d H_\nu^{(2)}(kr')}{dr'} \frac{1}{H_\nu^{(2)}(kr')}$,

a complex function

ψ = arg $\xi_\nu(kr')$

$f_{1\nu}^{(1)}(\Theta')$ = the Θ'-dependence of the components of the $HE_{1\nu}^{(1)}$mode

$f_{1\nu}^{(2)}(\Theta')$ = the Θ'-dependence of the components of the $HE_{1\nu}^{(2)}$mode

$G(\underline{r},\underline{r}')$ = Green's free space scalar function

J_n = Bessel function of first kind and order n

$F(\Theta,\Theta_o,kr')$ = radiation pattern function

DEPARTMENT OF ELECTRICAL ENGINEERING

Title : The Scalar Feed
part I: The boundary conditions

Authors : J.K.M. Jansen
Department of Mathematics
Technological University
Eindhoven

Netherlands

M.E.J. Jeuken
Technological University
Insulindelaan 2
Eindhoven
Netherlands

C.W. Lambrechtse
Technological University
Eindhoven
The Netherlands

Institute : Technological University Eindhoven

20th November, 1969

Abstract

The electromagnetic field in the grooves of a corrugated conical horn antenna has been investigated. The investigation started by modifying the boundaries of the grooves in such a way that they coincided with the spherical coordinate system. The purpose of the study has been to find the conditions under which E_ϕ, and $Z_o H_\phi$, are zero at the opening of the grooves, because in that case a symmetrical radiation pattern is obtained. This assertion will be proved in the second part of the paper. Under the condition that the width of the grooves is small compared with the wavelength, the following results are obtained. The dominant mode is a TM-mode and, neglecting the effect of the higher modes, we found that $E_\phi << E_r$. The second conclusion is that the depth of the grooves should be equal for all grooves not too close to the apex of the cone and equal to a quarter of a wavelength. In that case we found $Z_o H_\phi$, equal to zero.

1. Introduction

The illumination of a paraboloid reflector antenna depends on the properties of the feed used. In order to obtain a high efficiency it is necessary that the radiation pattern of the feed is as flat as possible and produces little spillover energy. Besides, it is desirable that the radiation pattern of the feed is symmetrical. Finally, the feed should possess a well-defined phase centre. For some applications, for instance for an antenna for line-on-sight communications it is necessary that the feed possesses the above properties in a large frequency range. A feed having all these properties has been proposed by Simmons and Kay [1] and they called it scalar feed. The scalar feed is a conical horn antenna with grooves, perpendicular to the wall of the horn. The flare angle of this feed can be small or large. The paper of Simmons and Kay gives only some experimental results without a theoretical explanation of the radiation pattern of the scalar feed. A shortcoming of this paper is that it does not contain useful design information concerning the scalar feed. This is mainly caused by the fact that a theoretical explanation of the radiation pattern of these feeds was not available at the moment of publication.

The investigation of the scalar feed is greatly facilitated by making a distinction between scalar feeds with a small and with a large flare angle. The radiation pattern of a scalar feed with small flare angle can be found by treating it as an open circular waveguide radiator and, if necessary, with a quadratic phase field distribution across the aperture. This has already been done by Jeuken and Kikkert [2]. They studied, both theoretically and experimentally, the radiation pattern of a conical horn antenna with small flare angle. The inner wall of the cone consisted of a corrugated boundary, composed of circumferential grooves. They found a

good agreement between the experimental and theoretical radiation pattern for the frequency range where the depth of the grooves was approximately a quarter of a wavelength. In het paper [2] the effect of the corrugations has been described by means of a impedance boundary condition, thus neglecting the detailed behaviour of the electromagnetic fields in the grooves.

Especially the frequency -dependent behaviour of the electromagnetic field in the grooves has not been taken into occount. Therefore it was not possible to find a theoretical explanation of the fact that the antenna has a symmetrical radiation pattern in the frequency range where the depth of the grooves is approximately a quarter of a wavelength.

Summarising, we may say that there is a need of a better understanding of the effect of the corrugation, especially as a function of the frequency. Moreover, it is desirable to compute the radiation pattern of the scalar feed with large flare angle in order to obtain useful design information concerning this feed. It is the purpose of the present paper to provide this information.

The paper consists two parts. In the first part the electromagnetic fields in the grooves will be thoroughly discussed and is the basis for the second part of the paper where the electromagnetic fields in the feed and the radiation pattern of the feed will be computed for various dimensions of the horn antennas.

Besides, a comparison with experimental results will be made and detailed information concerning the design of a scalar feed will be given.

2. The electromagnetic field in the groove.

The scalar feed is a conical horn antenna with grooves perpendicular to the wall of the horn (Fig.1). The computation of the electromagnetic field in a groove is a difficult task, because the boundaries of the groove do not coincide with a coordinate system in which Maxwell's equations can be easily solved. Therefore, we change the boundaries of the groove in such a way that they coincide with the spherical coordinate system. For a groove not to close the apex of the cone this is a good approximation.

One such groove is sketched in Fig. 2.

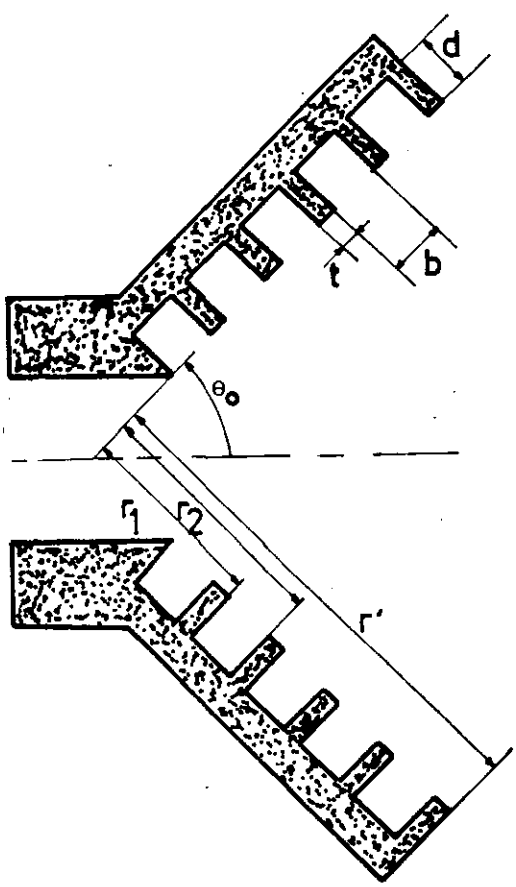

Fig. 1 The scalar feed.

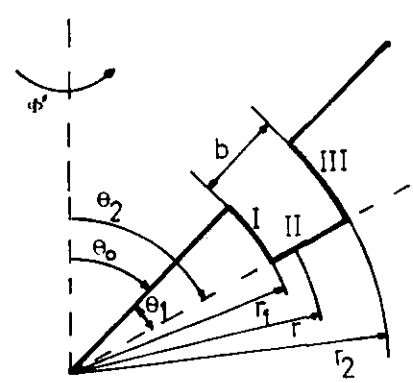

Fig. 2 Spherical groove and spherical coordinate system.

2.1 The TE-mode

2.1.1 The characteristic equation of the TE-mode

In this section we study the conditions under which a TE-mode can exist in a groove. The components of a TE-mode can be derived from the potential $F_r\ (r,\Theta,\phi)$ in the following way [3]:

$$E_r = 0 \qquad H_r = \frac{1}{j\omega\mu_o}\left(\frac{\partial^2}{\partial r^2} + k^2\right) F_r$$

$$E_\Theta = \frac{-1}{r\ \sin\Theta}\ \frac{\partial F_r}{\partial \phi} \qquad H_\Theta = \frac{1}{j\omega\mu_o}\ \frac{1}{r}\ \frac{\partial^2 F_r}{\partial r \partial \Theta} \qquad (1)$$

$$E_\phi = \frac{1}{r}\ \frac{\partial F_r}{\partial \Theta} \qquad H_\phi = \frac{1}{j\omega\mu_o}\ \frac{1}{r}\ \frac{1}{\sin\Theta}\ \frac{\partial^2 F_r}{\partial r \partial \phi}$$

The function $F_r\ (r,\Theta,\phi)$ has the form

$$F_r\ (r,\Theta,\phi) = kr\left(a_n j_n\ (kr) + b_n y_n\ (kr)\right)\left(c_{nm}\ P_n^m\ (\cos\ \Theta) + d_{nm} Q_n^m\ (\cos\ \Theta)\right)x$$

$$\left(e_m\ \cos\ m\phi + f_m\ \sin\ m\phi\right) \qquad (2)$$

In this expression the symbols used have the following meaning

$j_n\ (kr)$ and $y_n\ (kr)$	are the spherical Bessel function and the spherical Neumann function respectively.
$P_n^m\ (\cos\ \Theta)$ and $Q_n^m\ (\cos\ \Theta)$	are the associated Legendre functions of the first kind and the second kind respectively.
a_n, b_n, c_{nm}, d_{nm}, e_m and f_m	are constants which are determined by the boudary conditions and the strength of the electromagnetic field at the opening of the groove $\Theta = \Theta_o$.

The value of m depends on the way in which the electromagnetic field in the groove is excited. In most practical cases we have $m = 1$.

Application to the boundary condition $E_\Theta = 0$ for the boundaries I and III yields the equations

$$\begin{aligned} a_n\, j_n\,(kr_1) + b_n\, y_n\,(kr_1) &= 0 \\ a_n\, j_n\,(kr_2) + b_n\, y_n\,(kr_2) &= 0 \end{aligned} \tag{3}$$

These equations have a solution only if the determinant

$$\begin{vmatrix} j_n\,(kr_1) & y_n\,(kr_1) \\ j_n\,(kr_2) & y_n\,(kr_2) \end{vmatrix} = 0 \tag{4}$$

If there exists a solution of (4), then the value of n is known and (3) gives the value of the ratio a_n/b_n. A special solution of (4) exists if $k\,b = \pi$, then $n = 0$. The condition $E_\phi = 0$ for the boundaries I and III is satiesfied automatically. The third boundary condition, $E_\phi = 0$ for boundary II, yields:

$$\left[c_{nm}\, P_n^{m'}\,(\cos\Theta) + d_{nm}\, Q_n^{m'}\,(\cos\Theta) \right]_{\Theta = \Theta_2} = 0 \tag{5}$$

where the prime denotes differentiating with respect to $\cos\Theta$. From equation (5) we find the ratio c_{nm}/d_{nm}. From the considerations made so far still another conclusion can be drawn. The fact that e_m and f_m do not depend on the boundary conditions implies that two solutions F_r are possible; one with $f_m = 0$ and the other with $e_m = 0$. Summarising, we may say that if there exists a solution of (4), which means that a value of n can be found which satisfies (4), then there exists a TE-mode in the groove and the components of this electromagnetic field can be derived from the function

$$\begin{aligned} F_r\,(r,\Theta\,\phi) = kr\Big(y_n(kr_1)\, j_n(kr) - j_n(kr_1)\, y_n(kr)\Big)\Big(Q_n^{m'}\,(\cos\Theta_2)\, P_n^m\,(\cos\Theta) \\ - P_n^{m'}(\cos\Theta_2)\, Q_n^m\,(\cos\Theta)\Big)\Big(e_m \cos m\phi + f_m \sin m\phi\Big) \end{aligned} \tag{6}$$

If (4) has no solution, then $F_r(r,\theta\ \phi) = 0$ and no TE-mode can exist in the groove. The question whether (4) has a solution can be answered only after numerical analysis. However, in case the width of the groove is small compared with the wavelength, equation (4) can be simplified.

Using the abbreviations $kr_1 = x$ $kb = h$ and $kr_2 = x + h$ and applying the Taylor expansions

$$j_n(x + h) = j_n(x) + h\, j_n'(x) + O(h^2) \tag{7}$$

$$\text{and } y_n(x + h) = y_n(x) + h\, y_n'(x) + O(h^2) \tag{8}$$

we may replace the determinant in (4) by

$$h \begin{vmatrix} j_n(x) & y_n(x) \\ j_n'(x) & y_n'(x) \end{vmatrix} = hW\left(j_n(x), y_n(x)\right) = \frac{h}{x^2} \tag{9}$$

In this expression W represents the Wronskian [4]. So if $kb \ll 1$, then the determinant in (4) is never zero and (4) has no solutions, so that no TE-mode can exist in the groove.

A numerical analysis for finding the value of n as a function of kr_1 and kb is described in Appendix A. The results are given in Fig. 3. From these curves we see that n is approximately a linear function of kr_1. In conclusion we may say that no TE-mode exists in the groove, provided the width of the groove is smaller than half a wavelength.

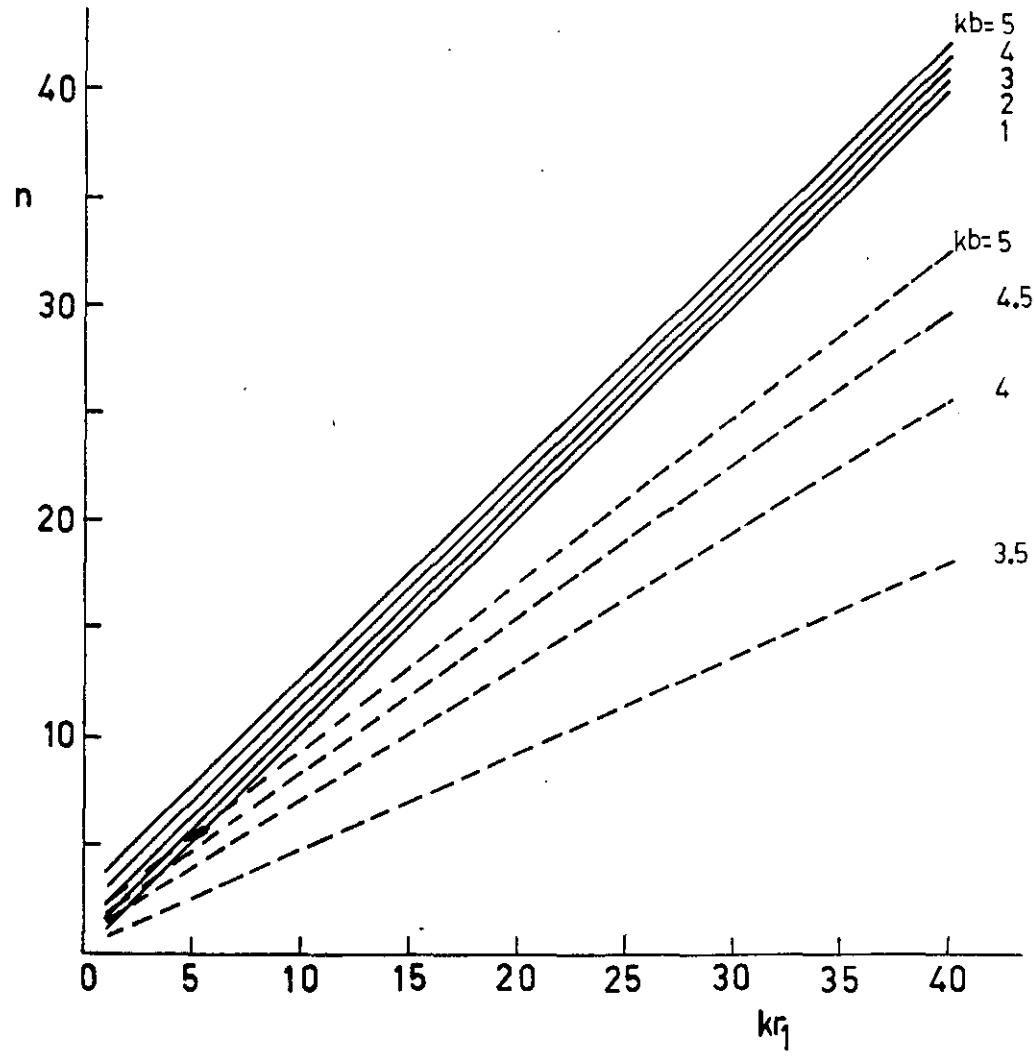

Fig. 3 n against kr_1 with kb as parameter

——— TM mode

----- TE mode

2.2 The TM-mode

2.2.1 The characteristic equation of the TM-mode

The TM-mode in the groove can be derived from the potential $A_r(r,\Theta,\phi)$ [3] by means of the following expressions

$$E_r = \frac{1}{j\omega\varepsilon_o}\left(\frac{\partial^2}{\partial r^2} + k^2\right)A_r \qquad H_r = 0$$

$$E_\Theta = \frac{1}{j\omega\varepsilon_o}\frac{1}{r}\frac{\partial^2 A_r}{\partial r\partial\Theta} \qquad H_\Theta = \frac{1}{r\sin\Theta}\frac{\partial A_r}{\partial\phi} \qquad (10)$$

$$E_\phi = \frac{1}{j\omega\varepsilon_o}\frac{1}{r\sin\Theta}\frac{\partial^2 A_r}{\partial r\partial\phi} \qquad H_\phi = -\frac{1}{r}\frac{\partial A_r}{\partial\Theta}$$

The function $A_r(r,\Theta,\phi)$ has the form

$$A_r(r,\Theta,\phi) = kr\left(a_n j_n(kr) + b_n y_n(kr)\right)\left(c_{nm}P_n^m(\cos\Theta) + d_{nm}Q_n^m(\cos\Theta)\right)x$$
$$\left(e_m\cos m\phi + f_m\sin m\phi\right) \qquad (11)$$

Application of the boundary condition $E_\phi = 0$ for the boundaries I and III gives rise to the next equation

$$\begin{vmatrix} j_n(kr_1) + kr_1\, j_n'(kr_1) & y_n(kr_1) + kr_1\, y_n'(kr_1) \\ j_n(kr_2) + kr_2\, j_n'(kr_2) & y_n(kr_2) + kr_2\, y_n'(kr_2) \end{vmatrix} = 0 \qquad (12)$$

Again, a special solution exists if $kb = \pi$; then $n = 0$

If there is a solution of (12), then $A_r(r,\Theta,\phi)$ has the following form

$$A_r(r,\Theta,\phi) = kr\left[\left(y_n(kr_1) + kr_1\, y_n'(kr_1)\right) j_n(kr) - \left(j_n(kr_1) + kr_1 j_n'(kr_1)\right)\right.$$
$$\left. x\, y_n(kr)\right]x$$
$$\left(Q_n^m(\cos\Theta_2)\, P_n^m(\cos\Theta) - P_n^m(\cos\Theta_2)\, Q_n^m(\cos\Theta)\right)x$$
$$\left(e_m\cos m\phi + f_m\sin m\phi\right) \qquad (13)$$

In the derivation of (13) use has been made of the boundary conditions $E_\phi = 0$ for $\Theta = \Theta_2$ and $E_r = 0$ for $\Theta = \Theta_2$. Of course, also in this case we see that (13) represents two solutions; one with $f_m = 0$ and the other with $e_m = 0$. Next, we assume that the width of the groove is small compared with the wavelength, so $kb \ll 1$. Applying the recurrence formulae [5]

$$f_n'(x) = \frac{n}{x} f_n(x) - f_{n+1}(x) \text{ and}$$
$$f_n'(x) = f_{n-1}(x) - \frac{n+1}{x} f_n(x), \tag{14}$$

Where $f_n(x)$ stands for $j_n(x)$, $y_n(x)$ respectively. Using the expansions (7) and (8) in (12) we obtain the equation

$$\left[-h\,x\right]\left[\frac{n(n+1)}{x} - x\right]\begin{vmatrix} j_{n+1}(x) & y_{n+1}(x) \\ j_n(x) & y_n(x) \end{vmatrix} = -\frac{h}{x^2}\left[n(n+1) - x^2\right] = 0 \tag{15}$$

So the solution of (12) for small values of kb is given by

$$n(n+1) = (kr_1)^2 \quad \text{or} \tag{16}$$
$$n = -\tfrac{1}{2} \pm \left[\tfrac{1}{4} + (kr_1)^2\right]^{\frac{1}{2}} \tag{17}$$

In the following considerations we shall omit the minus sign because it represents the same solution as the plus sign. From equation (17) we now see that $n \cong kr_1$ if $kr_1 \gg 1$ and $kb \ll 1$ (18) This result will be used in the following section. In conclusion, we see that a TM-mode can exist in the groove if its width is small compared to the wavelength.

A numerical analysis of equation (12), based on the method described in Appendix B gives n as a function of kr_1, for several values of kb. The results are also collected in Fig. 3. Note that n is approximately a linear function of kr_1, which is in agreement with (18).

2.2.2 The components of the electromagnetic field of the TM-mode

From the preceding considerations we know that only a TM-mode can exist in the groove, provided the width of the groove is smaller than half a wavelength. So it is now interesting to investigate the components of the electromagnetic field of this mode in more detail.

In the second part of the paper we shall prove that the boundary conditions $E_\phi = 0$ and $Z_o H_\phi = 0$ give rise to a symmetrical radiation pettern. Therefore, we shall first investigate the conditions under which $Z_o H_\phi = 0$. From the general expression of A_r (13) we see that $Z_o H_\phi = 0$, if we can find a value of Θ_o which satisfies the the equation

$$P_n^{m'}(\cos\Theta_o)\, Q_n^m(\cos\Theta_2) - P_n^m(\cos\Theta_2)\, Q_n^{m'}(\cos\Theta_o) = 0 \qquad (20)$$

where the prime means differentiating with respect to the argument. Useful insight into the behaviour of the groove can be obtained if for the moment we restrict our considerations to the case that $kb \ll 1$ and $kr_1 \gg 1$. Then we know from equation (18) that $n \gg 1$. So an asymptotic expansion of $P_n^m(\cos\Theta)$ and $Q_n^m(\cos\Theta)$ can be substituted in (20).

These expansions are [6]

$$P_n^m(\cos\Theta) = \frac{\Gamma(m+n+1)}{\Gamma(n+3/2)} \left(\tfrac{1}{2}\pi \sin\Theta\right)^{-\frac{1}{2}} \cos\left[(n+\tfrac{1}{2})\Theta - \frac{\pi}{4} - \frac{m\pi}{2}\right] + O\left(\frac{1}{n}\right) \qquad (21)$$

and

$$Q_n^m(\cos\Theta) = \frac{\Gamma(m+n+1)}{\Gamma(n+3/2)} \left(\frac{\pi}{2\sin\Theta}\right)^{\frac{1}{2}} \cos\left[(n+\tfrac{1}{2})\Theta + \frac{\pi}{4} + \frac{m\pi}{2}\right] + O\left(\frac{1}{n}\right) \qquad (22)$$

Substitution of (21) and (22) in (20) and using the relation [7]

$$L_n^{m'}(u) = \frac{-mu}{1-u^2} L_n^m(u) - \frac{1}{(1-u^2)^{\frac{1}{2}}} L_n^m(u) \text{ , where} \qquad (23)$$

$L_n^m(u)$ stands for $P_n^m(u)$ or $Q_n^m(u)$, we find after several algebraical manipulations

$$\tan(n+\tfrac{1}{2})\ (\Theta_2-\Theta_o) = \tan(n+\tfrac{1}{2})\Theta_o = (n+2)\ \tan\Theta_o \qquad (24)$$

The solution of this equation is

$$\Theta_l = \frac{\arctan\ (n+2)\ \tan\Theta_o\ +\ l\pi}{n+\tfrac{1}{2}} \qquad (25)$$

$l = 0, 1, 2, ..$

and for large value of n the approximation $\Theta_l \equiv \frac{\pi(2l+1)}{2n}$ is valid.

We know that $n \cong kr_l$, so $\Theta_l = \frac{\pi(2l+1)}{2\ kr_l}$ (26)

The depth of the groove s (Fig.4) is now given by

$$s = r_l\ \ \Theta_l = \frac{\pi(2l+1)}{2k} = \frac{\lambda}{4}\ (2l+1) \qquad (27)$$

and the important conclusion can be drawn that the depth of the groove is the same for all grooves that are far enough from the apex of the cone.

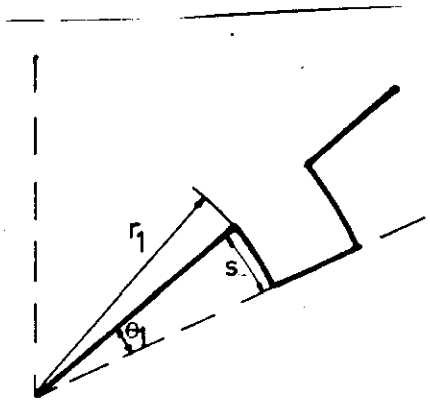

Fig. 4 Spherical groove with definition of s.

In the proof of (27) we have assumed that the flare angle Θ_o is large enough. So there is need for an exact computation of the depth of the groove under the condition that $Z_o H_\phi = 0$ at the opening of the groove. Such a computation can be carried out starting from the Runga-Kutta method and is described in some detail in Appendix C. The results are given in Fig. 5 and we may draw the following conclusions:

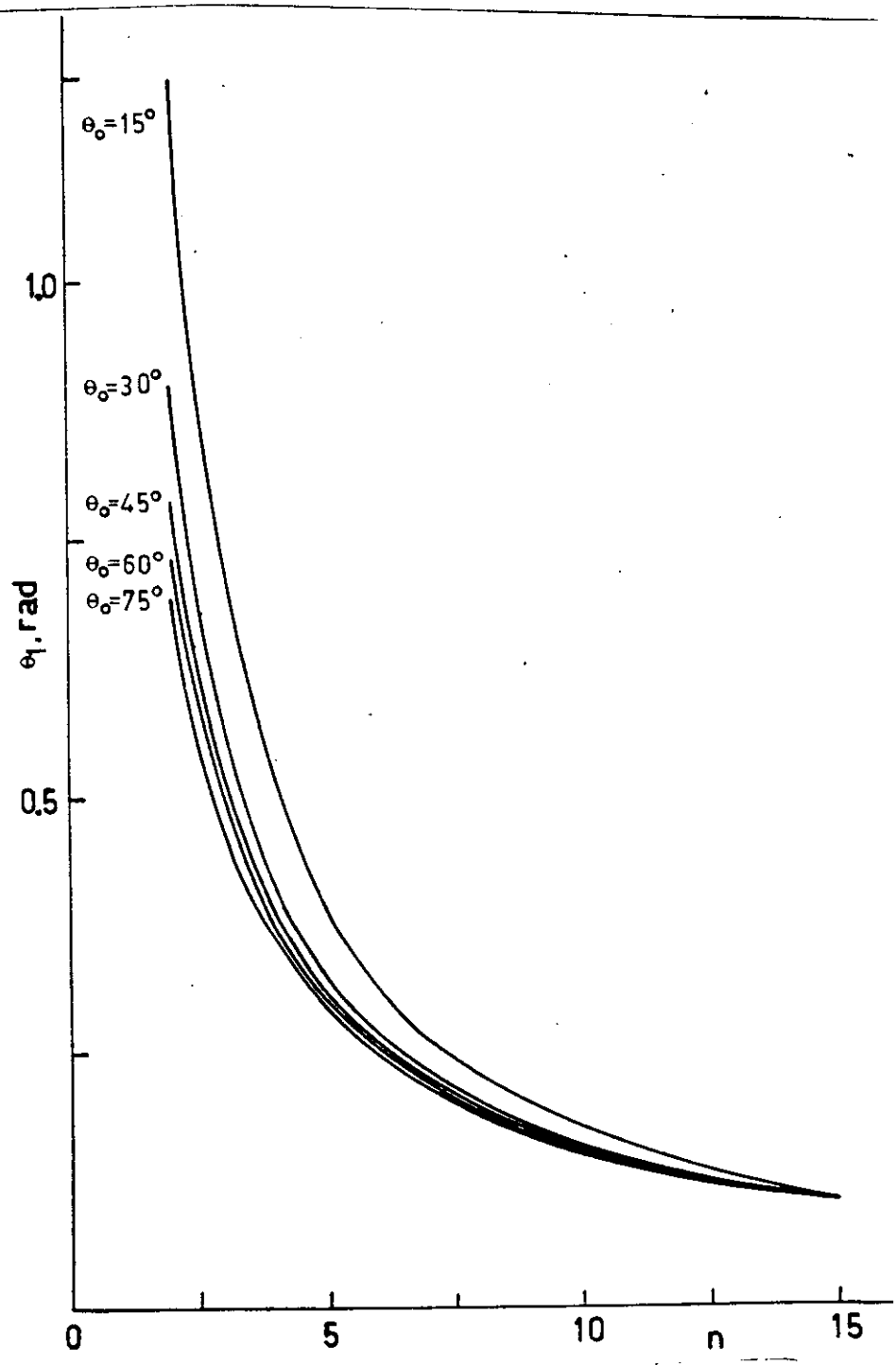

Fig. 5 Θ_1 against n with flare angle Θ_o as parameter.

(i) for grooves for which $n > 15$ the depth of the grooves can be found using (27);

(ii) for grooves for which $5 < n < 15$, the depth of the grooves is virtually independent of θ_o if $\theta_o < 30$;

(iii) for grooves characterized by a low value of n and a low value of θ_o we see that the depth of the grooves is a function of both n and θ_o.

So it is always possible to design the grooves in such a way that $Z_o H_\phi = 0$ at the opening of the grooves. Let us now study the electric field at the opening of the grooves. First we note that $E_\theta = 0$ if $Z_o H_\phi = 0$. For the case of $kb \ll 1$ some useful results can be derived from the general expressions (10) and (13). After a large amount of algebra we find

$$\frac{dA_r}{d(kr)} = \frac{(r-r_1)^2}{(kr_1)^2}\left[n(n+1) - (kr_1)^2\right] \qquad (28)$$

Using (10) en (15) we see that E_ϕ is zero in the groove. In the proof of (28) use has been made of the Taylor expansion (7). This expansion is not valid for low values of kr_1. So, for grooves in the vicinity of the apex of the cone E_ϕ cannot be neglected. Extensive calculations, which are not included, show that $E_\phi/E_r < 10^{-3}$ for $kr < 10$ and $kb \approx 1$.

2.2.3. The boundary conditions at the wall of the corrugated horn

The electromagnetic field at the opening of a narrow groove consists of the dominant TM-mode and evanescent modes. Experience teaches us that calculations concerning corrugated boundaries give useful results if the evaescent modes are neglected [8]. Accepting this approximation, we find that E_r is non-zero at the opening of the groove, while E_r is zero at the perfectly conducting dam between two successive grooves. $Z_o H_r$ is zero at the opening of a groove, but $Z_o H_r$ is non-zero at a dam, because currents on the dam in the ϕ -direction are possible. Currents in the r-direction are not possible if the width of the dams is small. This implies that $Z_o H_\phi$ is zero at a dam. Moreover, we choose the depth of the grooves in such a way that $Z_o H_\phi$ is zero at the opening of a groove. Finally, E_ϕ is zero at the dam and at the opening of the grooves. Suppose that there are many grooves per wavelength. Then we may formulate the following average boundary conditions at $\theta = \theta_o$

(i) E_r and $Z_o H_r$ are non-zero

(ii) E_ϕ and $Z_o H_\phi$ are zero

Starting from these boundary conditions the electromagnetic field in a corrugated horn will be calculated in the second part of the paper.

DEPARTMENT OF ELECTRICAL ENGINEERING

Title : The Scalar Feed
part II: The radiation pattern

Authors : M.E.J. Jeuken

Technological University

Insulindelaan 2

Eindhoven

Netherlands

C.W. Lambrechtse

Technological University

Eindhoven

Netherlands

Institute : Technological University Eindhoven

20th November 1969

3.1 Abstract

The electromagnetic field in the corrugated conical horn and its radiation pattern have been calculated for the case that the depth of the grooves was a quarter of a wavelength. The calculations are based on the boundary conditions, discussed in the first part of the paper. Several antennas have been constructed for verifying the theory. The conclusion is that a good agreement has been observed between the experimental and the theoretical results, at least for the frequency for which the depth of the grooves is a quarter of a wavelength. From the many measurements which have been carried out the following conclusions have been drawn. For large horn antennas with a flare angle smaller than 75^{o} there is a good agreement between experimental results and the calculations based on the assumption that $E_{\phi'}$ and $Z_{o}H_{\phi'}$ are zero at $\theta' = 0_{o}$, even at frequencies for which the depth of the grooves is not equal to a quarter of a wavelength. When the flare angle was smaller than 75^{o} and the antennas were short, again a resonable agreement between theory and experiment was found.

The paper concludes with rather detailed imformation concerning the design of the scalar feed. Besides, design charts are included.

3.2 The electromagnetic field in the corrugated conical horn

In the first part of this paper we have studied the boundary conditions which should be applied at the boundary $\theta' = \theta_o$ for the calculation of the electromagnetic field in the region bounded by $\theta' < \theta_o$. By inspection we see that neither a TE-mode nor a TM-mode can satisfy the boundary conditions. In fact, the electromagnetic field in the region $\theta' < \theta_o$ is a spherical hybrid mode. This mode can be understood as the sum of a TE-mode and a TM-mode. The components of this hybrid mode can be found by substituting

$$A_r(r',\theta',\phi') = A_1 P_\nu^1(\cos\theta') \cos\phi' \hat{H}_\nu^{(2)}(kr') \tag{29}$$

and

$$F_r(r',\theta',\phi') = A_2 P_\nu^1(\cos\theta') \sin\phi' \hat{H}_\nu^{(2)}(kr') \tag{30}$$

in equations (10) and (1) respectively and summing the TE part and TM part. In (29) and (30) $\hat{H}_\nu^{(2)}(kr')$ represents the spherical Hankel function of the second kind. It should be noted that primed coordinates are used for the description of the electromagnetic field in the horn. For the electromagnetic field in the grooves we have used unprimed coordinates. Finally, the coordinates of a point outside the horn antenna will be unprimed again. For the components of the spherical hybrid mode we find

$$E_{r'} = A_1 \frac{1}{j\omega\varepsilon_o} \frac{\nu(\nu+1)}{r'^2} P_\nu^1(\cos\theta') \cos\phi' \hat{H}_\nu^{(2)}(kr') \tag{31}$$

$$E_{\theta'} = \frac{A_1 Z_o \hat{H}_\nu^{(2)}(kr')}{r'} \left[\frac{dP^1{}_\nu(\cos\theta')}{d\theta'} \frac{1}{jk\hat{H}_\nu^{(2)}(kr')} \frac{d\hat{H}_\nu^{(2)}(kr')}{dr'} - \frac{A_2}{A_1 Z_o} \frac{1}{\sin\theta'} P_\nu^1(\cos\theta') \right] \cos\phi' \tag{32}$$

$$E_{\phi'} = \frac{A_1 Z_o \hat{H}_\nu^{(2)}(kr')}{r'} \left[-\frac{1}{\sin\theta'} P_\nu^1(\cos\theta') \frac{1}{jk\hat{H}_\nu^{(2)}(kr')} \frac{d\hat{H}_\nu^{(2)}(kr')}{dr'} + \frac{A_2}{A_1 Z_o} \frac{dP_\nu^1(\cos\theta')}{d\theta'} \right] \sin\phi' \qquad (33)$$

$$Z_o H_{r'} = \frac{Z_o A_2}{j\omega\mu_o} \frac{\nu(\nu+1)}{r'^2} P_\nu^1(\cos\theta') \sin\phi' \hat{H}_\nu^{(2)}(kr') \qquad (34)$$

$$Z_o H_{\theta'} = \frac{A_1 Z_o \hat{H}_\nu^{(2)}(kr')}{r'} \left[\frac{A_2}{A_1 Z_o} \frac{dP_\nu^1(\cos\theta')}{d\theta'} \frac{1}{j\,k\hat{H}_\nu^{(2)}(kr')} \frac{d\hat{H}_\nu^{(2)}(kr')}{dr'} - \frac{1}{\sin\theta'} P_\nu^1(\cos\theta') \right] \sin\phi' \qquad (35)$$

$$Z_o H_{\phi'} = \frac{A_1 Z_o \hat{H}_\nu^{(2)}(kr')}{r'} \left[-\frac{dP_\nu^1(\cos\theta')}{d\theta'} + \frac{A_2}{A_1 Z_o} \frac{1}{\sin\theta'} P_\nu^1(\cos\theta') \times \frac{1}{jk\hat{H}_\nu^{(2)}(kr')} \frac{d\hat{H}_\nu^{(2)}(kr')}{dr'} \right] \cos\phi' \qquad (36)$$

In the expressions (31) to (36) incl. the unknown quantities are $\frac{A_1}{A_2}$ and ν, and can be found after applying the boundary conditions $E_{\phi'} = 0$ and $Z_o H_{\phi'} = o$ for $\theta' = \theta_o$. From these conditions we find that

$$\frac{A_2}{A_1 Z_o} = \pm 1 \qquad (37)$$

and we observe that the simple solution (37) is possible because $Z_o H_{\phi'} = 0$, which is the case for grooves with a depth equal to a quarter of a wavelength.

So two modes with the same ϕ'-dependence, but different θ'-dependence can exist in the corrugated conical horn. The mode for which $A_2 = Z_o A_1$ is called the $HE_{1\nu}^{(1)}$-mode, while the other is the $HE_{1\nu}^{(2)}$-mode.

Substitution of (37) in the equation $Z_o H_{\phi'} = 0$ yields the characteristic equations

$$\left[\frac{dP_\nu^1(\cos\theta')}{d\theta'} \pm \frac{1}{\sin\theta'} P_\nu^1(\cos\theta')\, \xi_\nu(kr')\right]_{\theta'=\theta_o} = 0 \qquad (38)$$

The function $\xi_\nu(kr') = \frac{1}{jk} \frac{d\hat{H}_\nu^{(2)}(kr')}{dr'} \frac{1}{\hat{H}_\nu^{(2)}(kr')}$ and is a complex function

Using the asymptotic expansion of $\hat{H}_\nu^{(2)}(kr')$ we see that $\lim_{kr'\to\infty} \xi_\nu(kr') = -1$

For this case we have solved (38) for the lowest value ν. The results are plotted in Fig. 6. For purposes of comparison we have also plotted the value of ν of the $TE_{1\nu}$-mode and the $TM_{1\nu}$-mode in a perfectly conducting conical horn. The function $\xi_\nu(kr')$ has also been computed for finite values of kr' and for those values of ν which occur for the $HE_{1\nu}^{(1)}$-mode in a very large horn and with flare angles $\theta_o = 15^o$, 30^o, 45^o, 60^o and 75^o. The results are plotted in Fig. 7 and show that the approximation $\xi_\nu(kr') \cong -1$ is also valid for rather low values of kr'. Let us now calculate the transverse electric and magnetic field components of the $HE_{1\nu}^{(1)}$-mode.

Substitution of $A_1 Z_o = A_2$ in (32) to (36) incl. gives

$$E_{\theta'} = -\frac{A_1 Z_o \hat{H}_\nu^{(2)}(kr')}{r'} f_{1\nu}^{(1)}(\theta') \cos\phi' \qquad (39)$$

$$E_{\phi'} = \frac{A_1 Z_o \hat{H}_\nu^{(2)}(kr')}{r'} f_{1\nu}^{(1)}(\theta') \sin\phi' \qquad (40)$$

$$Z_o H_{\theta'} = -\frac{A_1 Z_o \hat{H}_\nu^{(2)}(kr')}{r'} f_{1\nu}^{(1)}(\theta') \sin\phi' \qquad (41)$$

$$Z_o H_{\phi'} = -\frac{A_1 Z_o \hat{H}_\nu^{(2)}(kr')}{r'} f_{1\nu}^{(1)}(\theta') \cos\phi' \qquad (42)$$

$$\text{with } f_{1\nu}^{(1)}(\theta') = \frac{dP_\nu^1(\cos\theta')}{d\theta'} + \frac{1}{\sin\theta'} P_\nu^1(\cos\theta') \qquad (43)$$

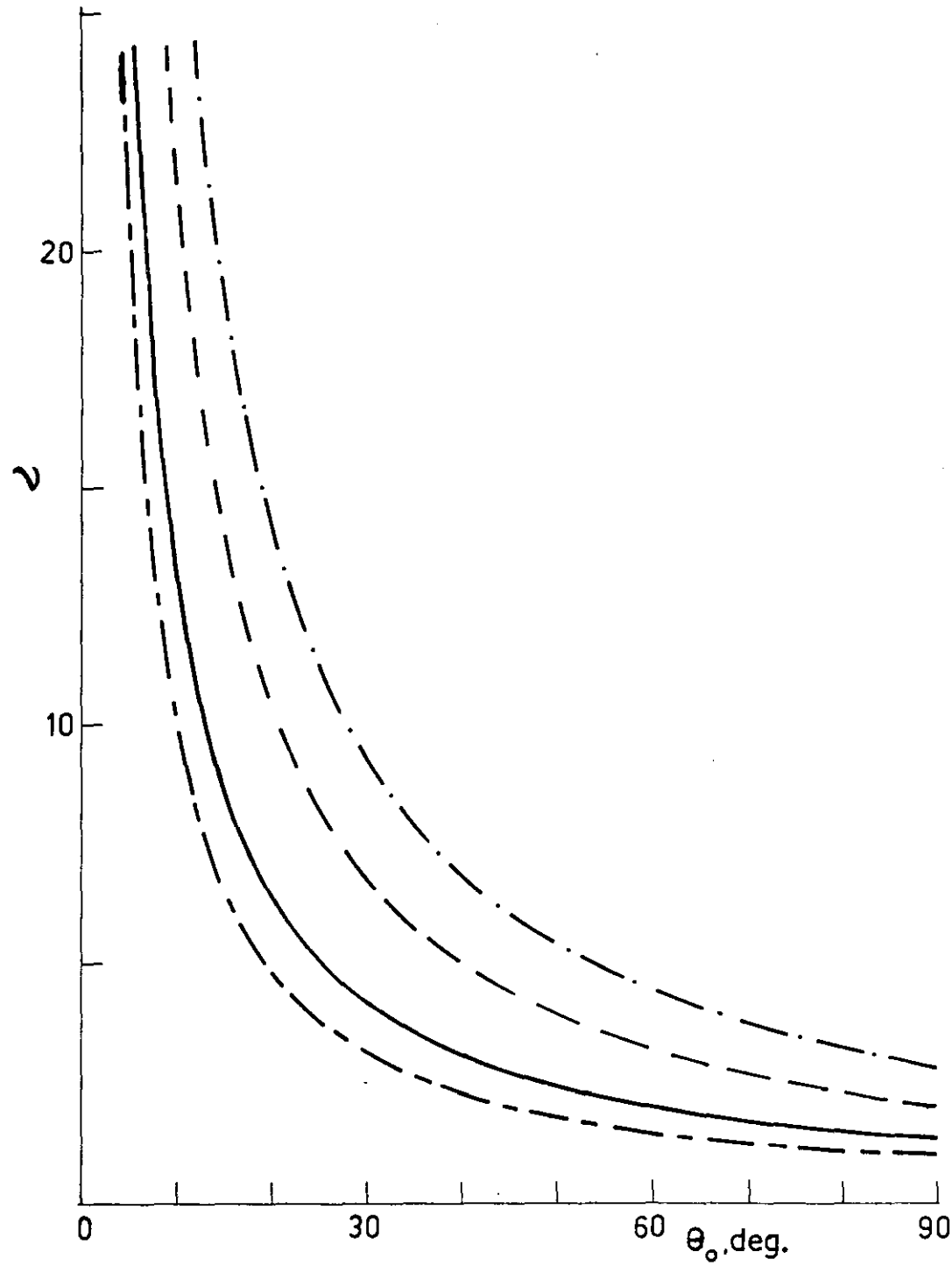

Fig. 6 ν against flare angle θ_o for several modes.

— - — - $TE_{1\nu}$ mode in perfectly conducting conical horn antenna

- - - - - - $TM_{1\nu}$ mode in perfectly conducting conical horn antenna

———— $HE_{1\nu}^{(1)}$ mode in corrugated conical horn antenna

-.-.-.-.-. $HE_{1\nu}^{(2)}$ mode in corrugated conical horn antenna

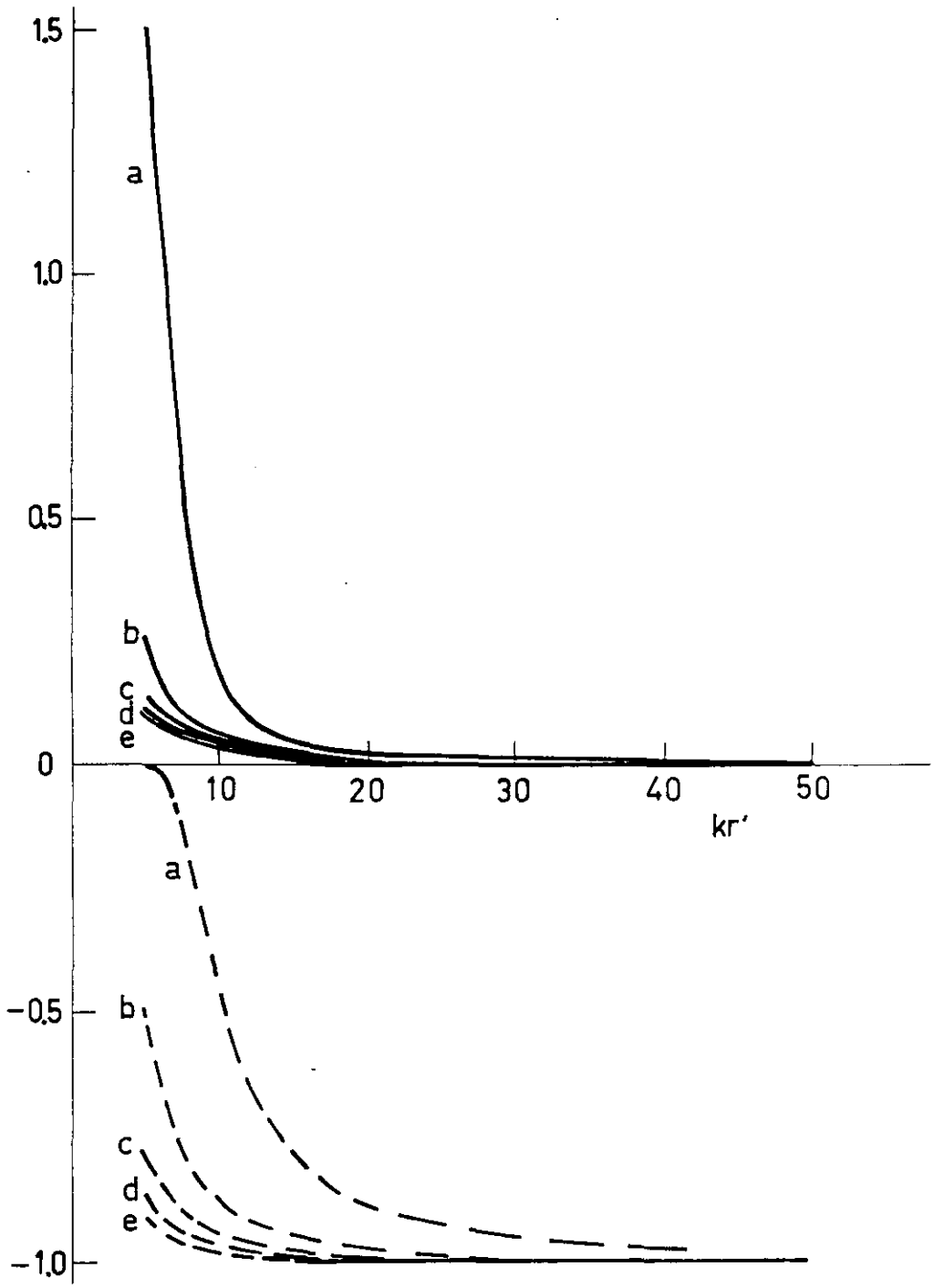

Fig. 7 Re $\xi_\nu(kr')$ and Im $\xi_\nu(kr')$ against kr' with ν as parameter

——— Im $\xi_\nu(kr')$

---------- Re $\xi_\nu(kr')$

a : $\Theta_o = 15^\circ$; $\nu = 8.74$

b : $\Theta_o = 30^\circ$; $\nu = 4.19$

c : $\Theta_o = 45^\circ$; $\nu = 2.71$

d : $\Theta_o = 60^\circ$; $\nu = 2.00$

e : $\Theta_o = 75^\circ$; $\nu = 1.59$

Comparing (43) with (38) we see that all the transverse electric and magnetic components are zero for $\theta' = \theta_o$. Especially the fact that $E_{\theta'} = o$ for $\theta' = \theta_o$ is important, because in a conical horn antenna with perfectly conducting walls both $Z_o H_{\phi'}$ and $E_{\theta'}$ are non-zero and give rise to the high side-lobes in the E-plane [2]. In Fig.8 the function $f_{1\nu}^{(1)}(\theta')$ has been plotted for the same values of ν as in Fig.7. The main conclusion is that the function $f_{1\nu}^{(1)}(\theta')$ has a maximum for $\theta' = 0$.

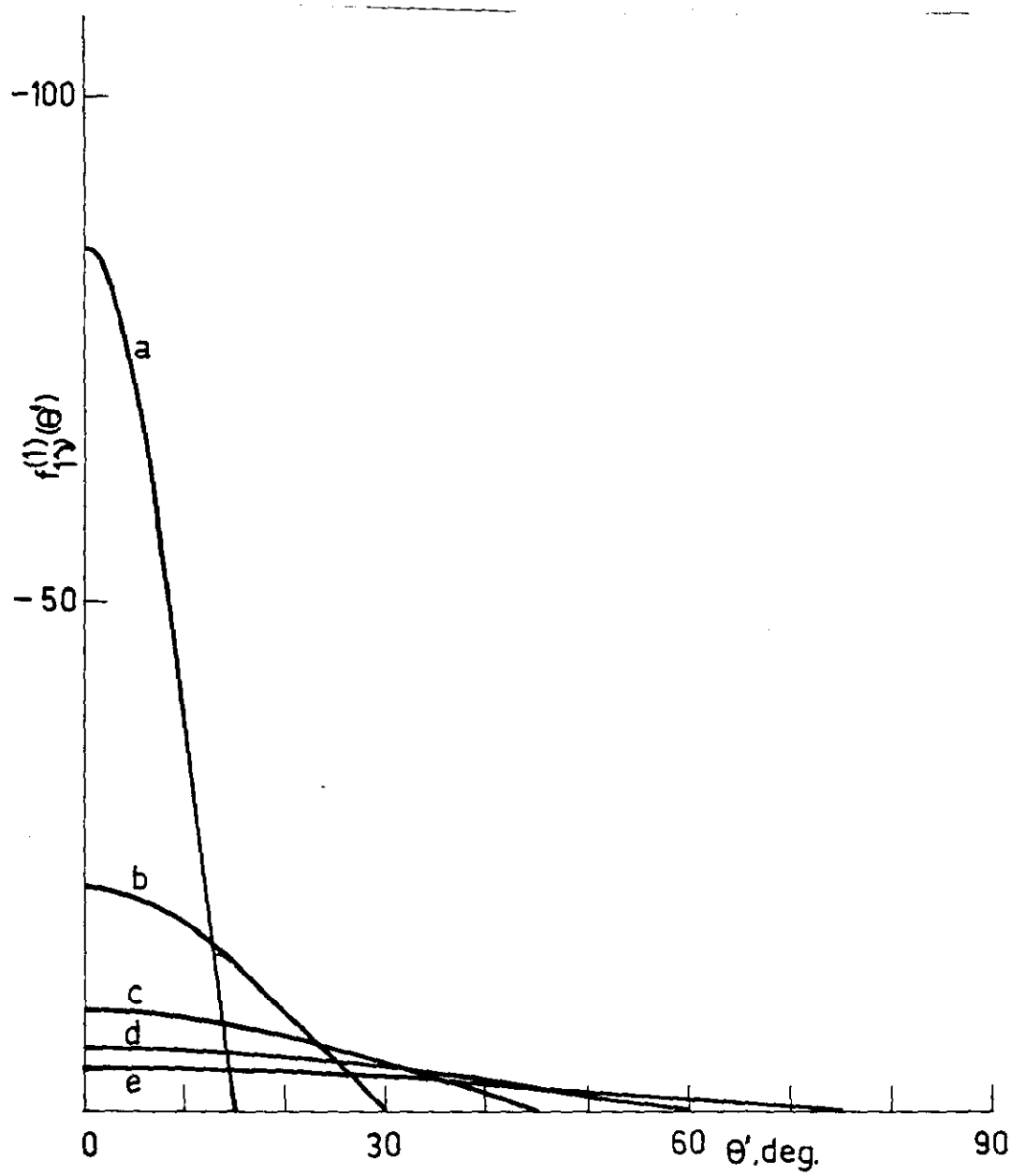

Fig. 8 $f_{1\nu}^{(1)}(\theta')$ against θ' with ν as parameter

a : $\theta_o = 15^o$; $\nu = 8.74$

b : $\theta_o = 30^o$; $\nu = 4.19$

c : $\theta_o = 45^o$; $\nu = 2.71$

d : $\theta_o = 60^o$; $\nu = 2.00$

e : $\theta_o = 75^o$; $\nu = 1.59$

For the H $E_{1\nu}^{(2)}$-mode we find

$$E_{\theta'} = -\frac{A_1 Z_o \hat{H}_\nu^{(2)}(kr')}{r'} f_{1\nu}^{(2)}(\theta') \cos\phi' \tag{44}$$

$$E_{\phi'} = -\frac{A_1 Z_o \hat{H}_\nu^{(2)}(kr')}{r'} f_{1\nu}^{(2)}(\theta') \sin\phi' \tag{45}$$

$$Z_o H_{\theta'} = \frac{A_1 Z_o \hat{H}_\nu^{(2)}(kr')}{r'} f_{1\nu}^{(2)}(\theta') \sin\phi' \tag{46}$$

$$Z_o H_{\phi'} = -\frac{A_1 Z_o \hat{H}_\nu^{(2)}(kr')}{r'} f_{1\nu}^{(2)}(\theta') \cos\phi' \tag{47}$$

$$\text{with } f_{1\nu}^{(2)}(\theta') = \frac{dP_\nu^1(\cos\theta')}{d\theta'} - \frac{1}{\sin\theta'} P_\nu^1(\cos\theta') \tag{48}$$

The function $f_{1\nu}^{(2)}(\theta')$ has been plotted in Fig. 9 for the same values of ν as in Fig. 8. We observe that $f_{1\nu}^{(2)}(0) = 0$. In the next section we shall prove that the radiation pattern of the $HE_{1\nu}^{(2)}$-mode has a dip for $\theta' = 0$.

So this mode is not suitable for antenna applications.

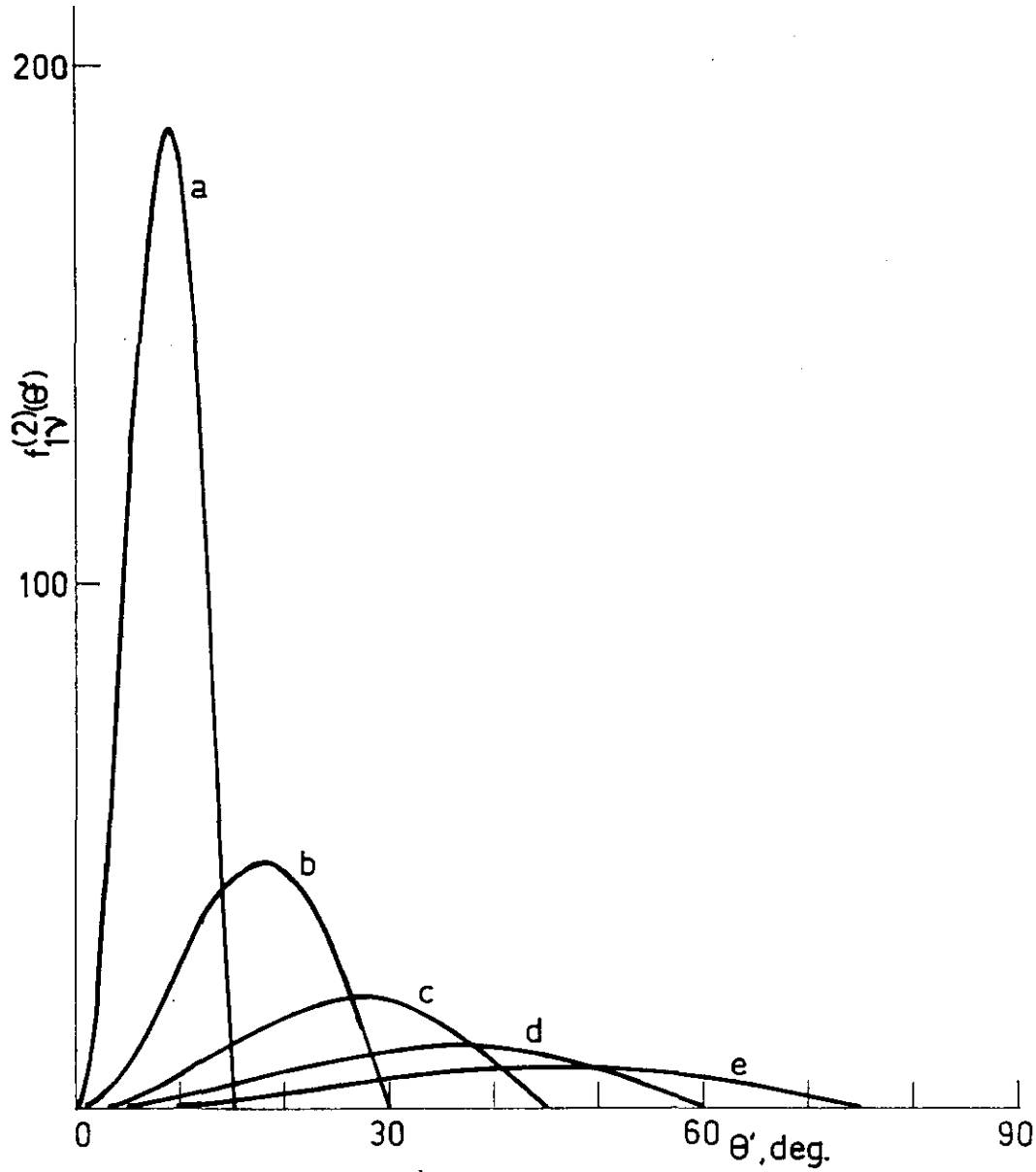

Fig. 9 $f_{1\nu}^{(2)}(\theta')$ against θ' with ν as parameter

a : $\theta_o = 15^\circ$; $\nu = 19.12$

b : $\theta_o = 30^\circ$; $\nu = 9.32$

c : $\theta_o = 45^\circ$; $\nu = 6.06$

d : $\theta_o = 60^\circ$; $\nu = 4.43$

e : $\theta_o = 75^\circ$; $\nu = 3.45$

4. The radiation pattern of the corrugated conical horn antenna

4.1 Computation of the radiation pattern

The electromagnetic field of a radiating conical horn antenna can be found from the following representation theorem. [13]

$$\underline{E}(\underline{r}) = \text{curl}_p \int_{S_A} \left[\underline{n}' \times \underline{E}(\underline{r}')\right] G(\underline{r},\underline{r}')dS + \frac{1}{j\omega\varepsilon_0} \text{curl}_p \text{curl}_p \int_{S_A} \left[\underline{n}' \times \underline{H}(\underline{r}')\right] G(\underline{r},\underline{r}')dS \tag{49}$$

$$\underline{H}(\underline{r}) = \text{curl}_p \int_{S_A} \left[\underline{n}' \times \underline{H}(\underline{r}')\right] G(\underline{r},\underline{r}')dS - \frac{1}{j\omega\mu_0} \text{curl}_p \text{curl}_p \int_{S_A} \left[\underline{n}' \times \underline{E}(\underline{r}')\right] G(\underline{r},\underline{r}')dS \tag{50}$$

$$\text{with } G(\underline{r},\underline{r}') = \frac{1}{4\pi} \frac{e^{-jk|\underline{r}-\underline{r}'|}}{|\underline{r}-\underline{r}'|}$$

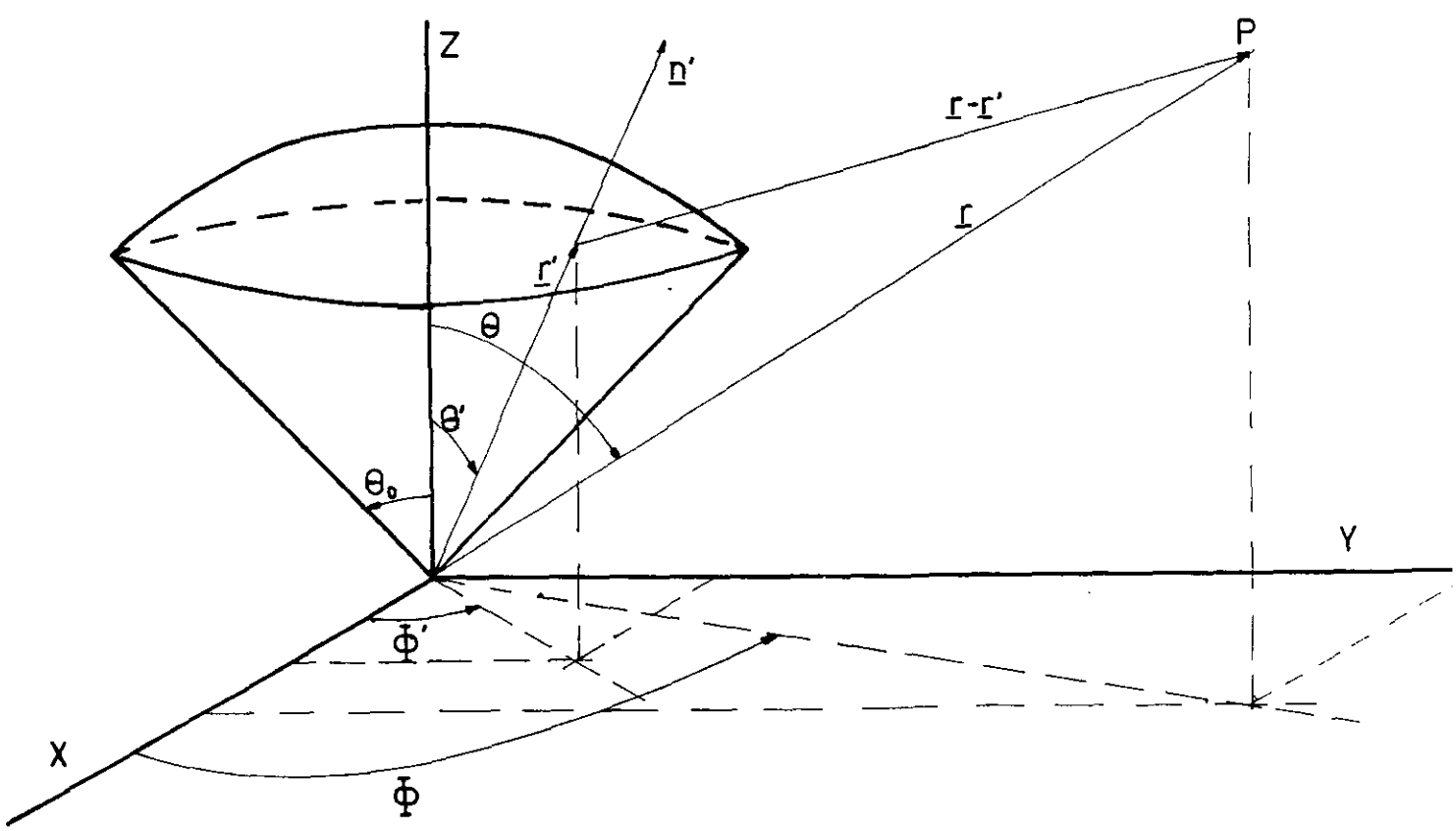

Fig. 10 Conical horn antenna with coordinate system.

In these expressions we have assumed that the outside of the horn antenna is perfectly conducting and no currents flow on the outside of the antenna. The aperture S_A is part of a sphere with radius r'.

The far field approximation gives

$$E_\theta(r,\theta,\phi) = \frac{e^{-jkr}}{r} \frac{jk}{4\pi} \int_{S_A} \left[\left\{ E_{\phi'} \cos\theta' - Z_o H_{\theta'} \cos\theta \right\} \sin(\phi - \phi') + \right.$$

$$\left. + \left\{ E_{\theta'} + Z_o H_{\phi'} \cos\theta' \cos\theta \right\} \cos(\phi - \phi') + Z_o H_{\phi'} \sin\theta \sin\theta' \right] \times$$

$$\exp\left[+ jkr' \left\{ \cos\theta \cos\theta' + \sin\theta \sin\theta' \cos(\phi - \phi') \right\} \right] (r')^2 \sin\theta' d\theta' d\phi' \quad (51)$$

$$E_\phi(r,\theta,\phi) = \frac{e^{-jkr}}{r} \frac{jk}{4\pi} \int_{S_A} \left[-\left\{ E_{\theta'} \cos\theta + Z_o H_{\phi'} \cos\theta' \right\} \sin(\phi - \phi') + \right.$$

$$\left. + \left\{ - Z_o H_{\theta'} + E_{\phi'} \cos\theta' \cos\theta \right\} \cos(\phi - \phi') + E_{\phi'} \sin\theta \sin\theta' \right] \times$$

$$\exp\left[+ jkr' \left\{ \cos\theta \cos\theta' + \sin\theta \sin\theta' \cos(\phi - \phi') \right\} \right] (r')^2 \sin\theta' d\theta' d\phi' \quad (52)$$

Substituting (39) to (42) incl. in (51) and (52) and using the relation

$$e^{jkr' \sin\theta \sin\theta' \cos(\phi-\phi')} = J_o(kr'\sin\theta\sin\theta') + \sum_{n=1}^{\infty} 2j^n J_n(kr'\sin\theta \sin\theta') \cos n(\phi-\phi') \quad (53)$$

we obtain

$$E_\theta = -\frac{jk}{4} \frac{e^{-jkr}}{r} A_1 Z_o \frac{\hat{H}_\nu^{(2)}(kr')}{r'} (r')^2 \cos\phi \; F(\theta,\theta_o,kr') \quad (54)$$

and

$$E_\phi = \frac{jk}{4} \frac{e^{-jkr}}{r} A_1 Z_o \frac{\hat{H}_\nu^{(2)}(kr')}{r'} (r')^2 \sin\phi \; F(\theta,\theta_o,kr') \quad (55)$$

with

$$F(\theta,\theta_o,kr') = \int_o^{\theta_o} \left[\left\{ \cos\theta + \cos\theta' \right\} \left\{ J_o(kr' \sin\theta \sin\theta') + J_2(kr' \sin\theta \sin\theta') \right\} + \right.$$

$$+ \left\{ 1 + \cos\theta \cos\theta' \right\} \left\{ J_o(kr' \sin\theta \sin\theta') - J_2(kr' \sin\theta \sin\theta') \right\} +$$

$$\left. + 2j \sin\theta \sin\theta' J_1(kr'\sin\theta\sin\theta') \right] f_{1\nu}^{(1)}(\theta') \exp\left[jkr' \cos\theta\cos\theta' \right] \sin\theta' d\theta' \quad (56)$$

From the equation (54) and (55) we derive that $|E_\theta|^2 + |E_\phi|^2$ is independent of ϕ. It should be noted that the same result has already been found in [2] for the case that the flare angle was small. So the radiation pattern of a corrugated conical horn antenna is symmetrical, provided the depth of the grooves is a quarter of a wavelength, because in that case $Z_o H_{\phi'} = 0$.

Substitution of (44) to (47) incl. in (51) and (52) shows that the $HE_{1\nu}^{(2)}$-mode has also a symmetrical radiation pattern, but with a dip for $\theta = 0$. This type of radiation pattern is not studied in this paper.

From equations (54) and (55) we derive that

$$\left|\frac{E_\theta(\theta,\theta_o,kr')}{E(0,\theta_o,kr')}\right| = \left|\frac{E_\phi(\theta,\theta_o,kr')}{E_\phi(0,\theta_o,kr')}\right| = \left|\frac{F(\theta,\theta_o,kr')}{F(0,\theta_o,kr')}\right| \qquad (57)$$

The function $20\log\left|\frac{F(\theta,\theta_o,kr')}{F(0,\theta_o,kr')}\right|$ has been calculated for several values of θ_o and kr'. From these calculations the beamwidth has been derived as a function of kr' for $\theta_o = 15^\circ$, 30°, 45°, 60° and 75°. The results are plotted in Fig.11 to Fig.15 incl. It should be noted that these results are found under the assumption that the function $\xi_\nu(kr') = -1$. However, this is not valid for small values of kr' as can be seen from Fig.7. For the case that $\xi_\nu(kr') \neq -1$ we see that (38) has no real solutions for ν. As (38) will have to give real values of ν, we assume that

$$\frac{A_2}{A_1 Z_o} = \exp -j\left[\psi - \pi\right]$$

with $\psi = \arg \xi_\nu(kr')$. Again it is still possible to satisfy the condition $Z_o H_{\phi'} = 0$. However, then $E_{\phi'} \neq 0$, which is in agreement with the results of the first part of this paper (equation (28) et seqq.)

To satisfy the boundary condition $E_{\phi'} \neq 0$ one needs a set of infinite modes. So the assumption (58) can give only an approximation of the aperture fields of small corrugated horn antennas. Starting from (58) several computations of the radiation pattern of small corrugated horns have been carried

out. The conclusion is that there exists a slight difference between the E-plane pattern and the H-plane pattern. This difference has also been found experimentally. [14] . However, the difference is so small that it does not impair the performance of the antenna. So for a practical design of these antennas one can use the average value of the beamwidths in the E-plane and the H-plane.

For purposes of illustration the results of calculations based on (58) and those based on the assumption $\xi_\nu(kr') = -1$ are included in Fig.16. The results are in agreement with the previous conclusions. So it was decided to use the aperture fields (39) to (42) incl. also for the calculation of the radiation pattern of small antennas.

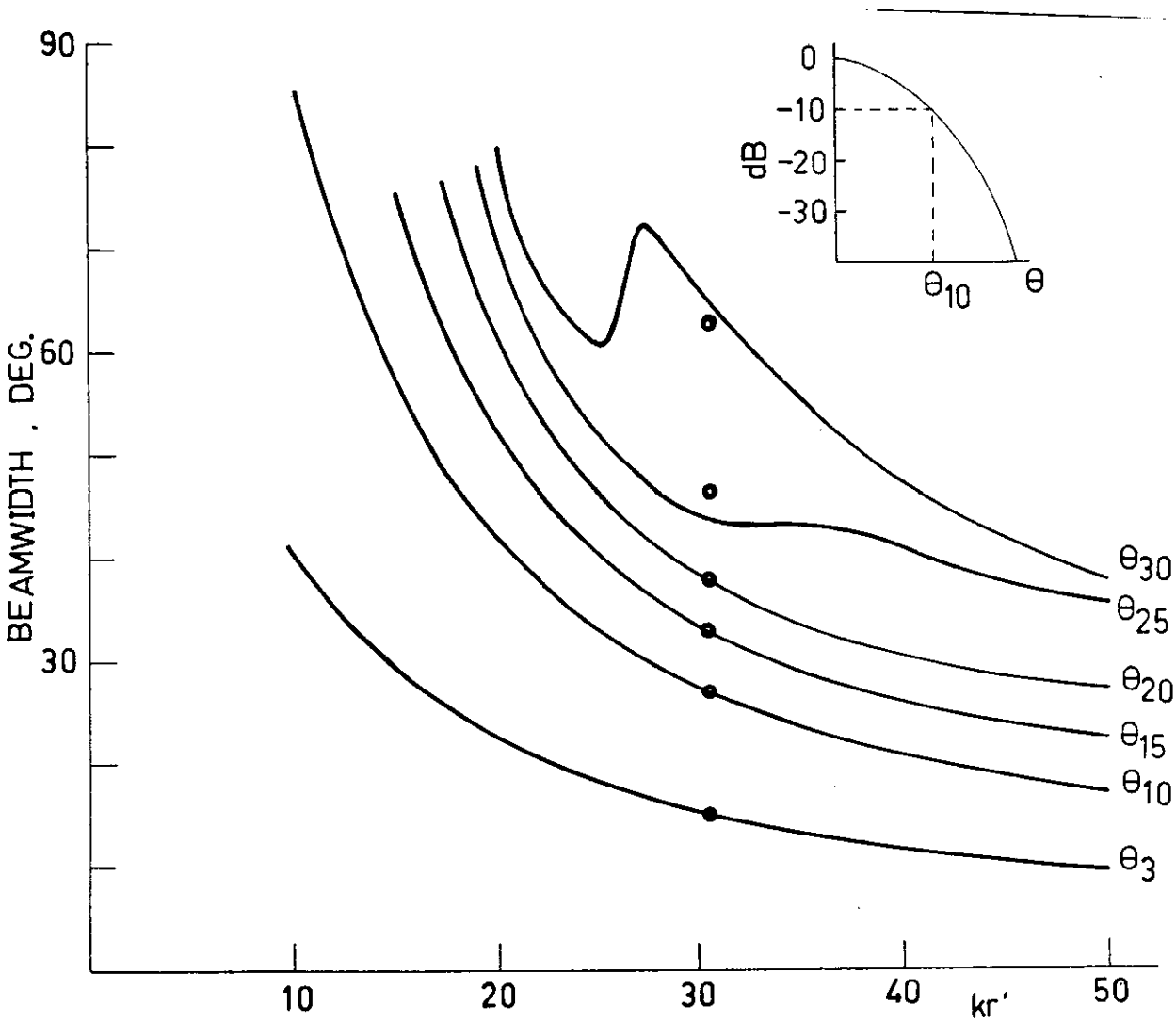

Fig. 11 Beamwidth against kr' for $\theta_o = 15^o$; dots indicate experimental results obtained with antenna 1 at a frequency of 8.33 GHz ; diameter waveguide is 28 mm.

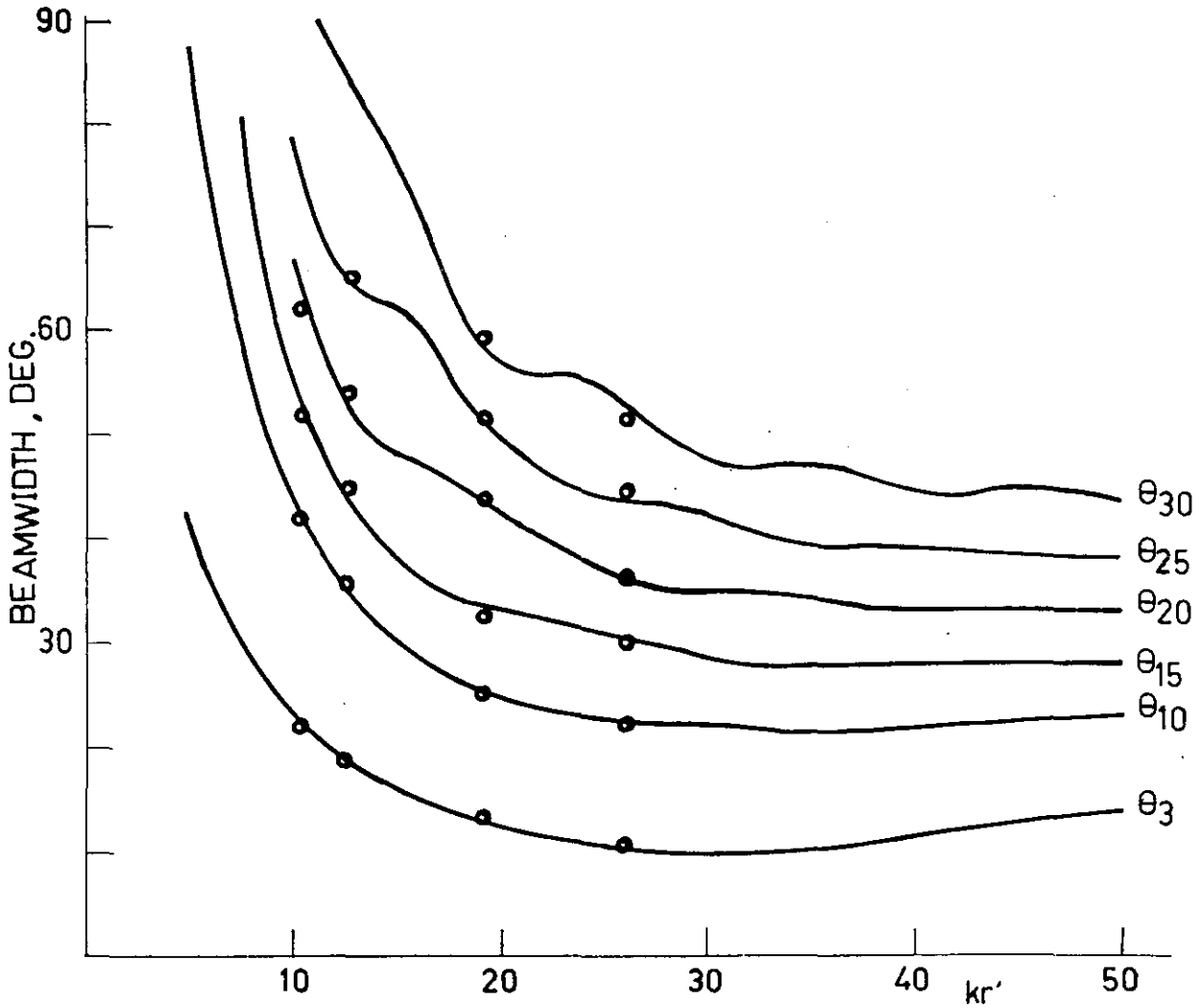

Fig. 12 Beamwidth against kr' for $\theta_o = 30^o$; dots indicate experimental results obtained with the antennas 2, 3, 4 and 5 at a frequency of 14 GHz.

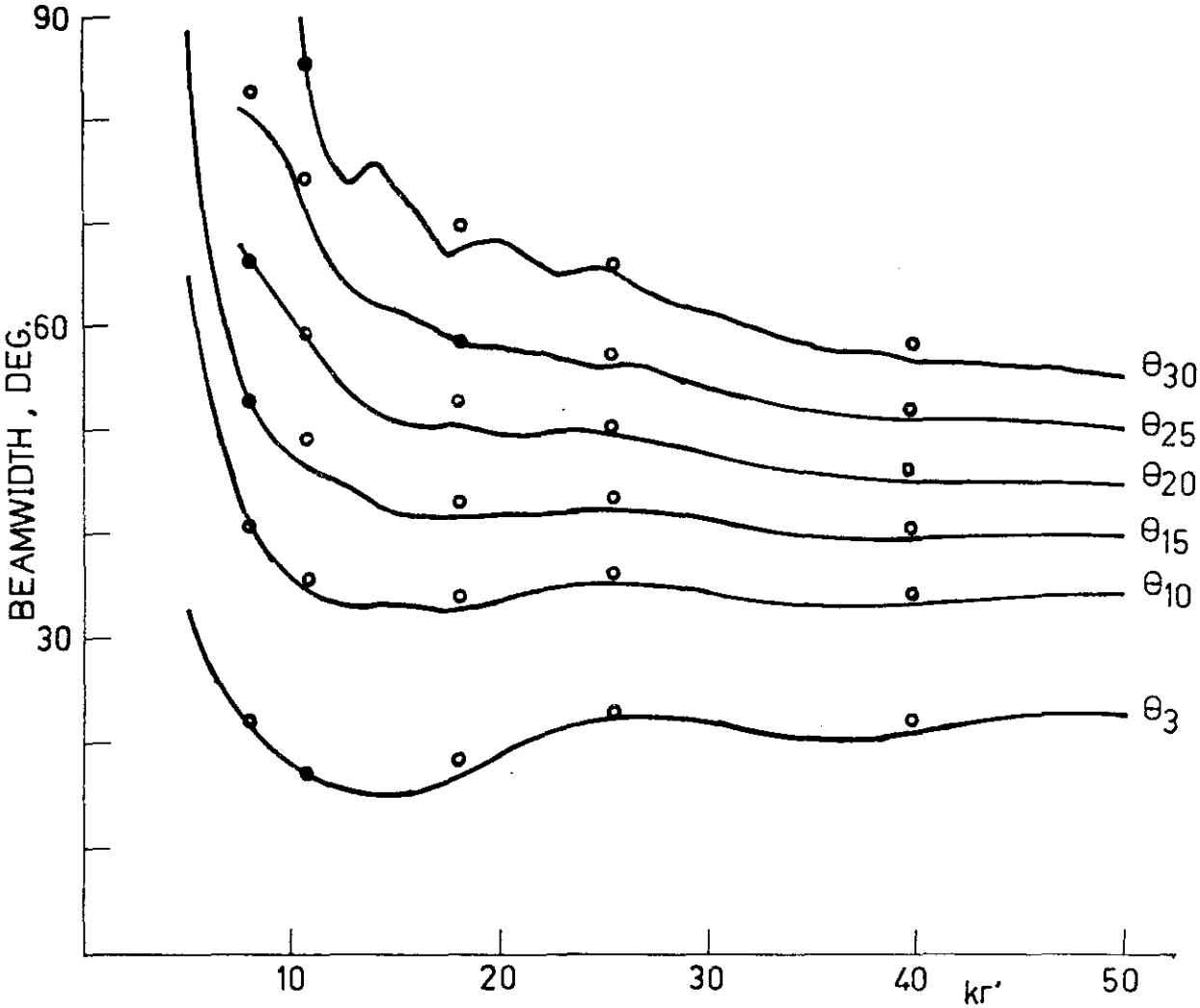

Fig. 13 Beamwidth against kr' for $\Theta_o = 45^\circ$; dots indicate experimental results obtained with the antennas 6, 7, 8, 9 and 10 at a frequency of 14 GHz.

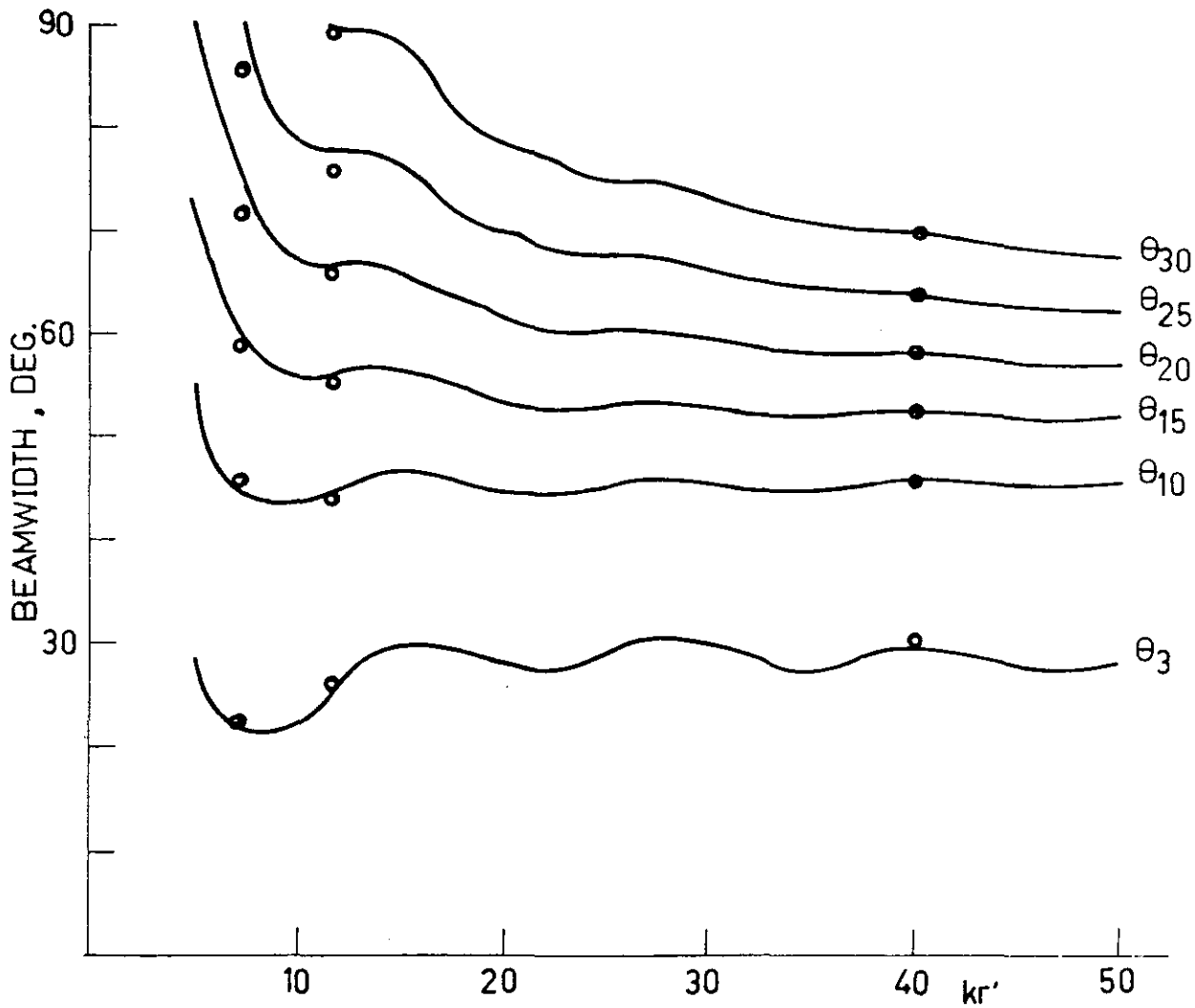

Fig. 14 Beamwidth against kr' for $\theta_o = 60^0$; dots indicate experimental results obtained with the antennas 11, 12 and 13 at a frequency of 14 GHz.

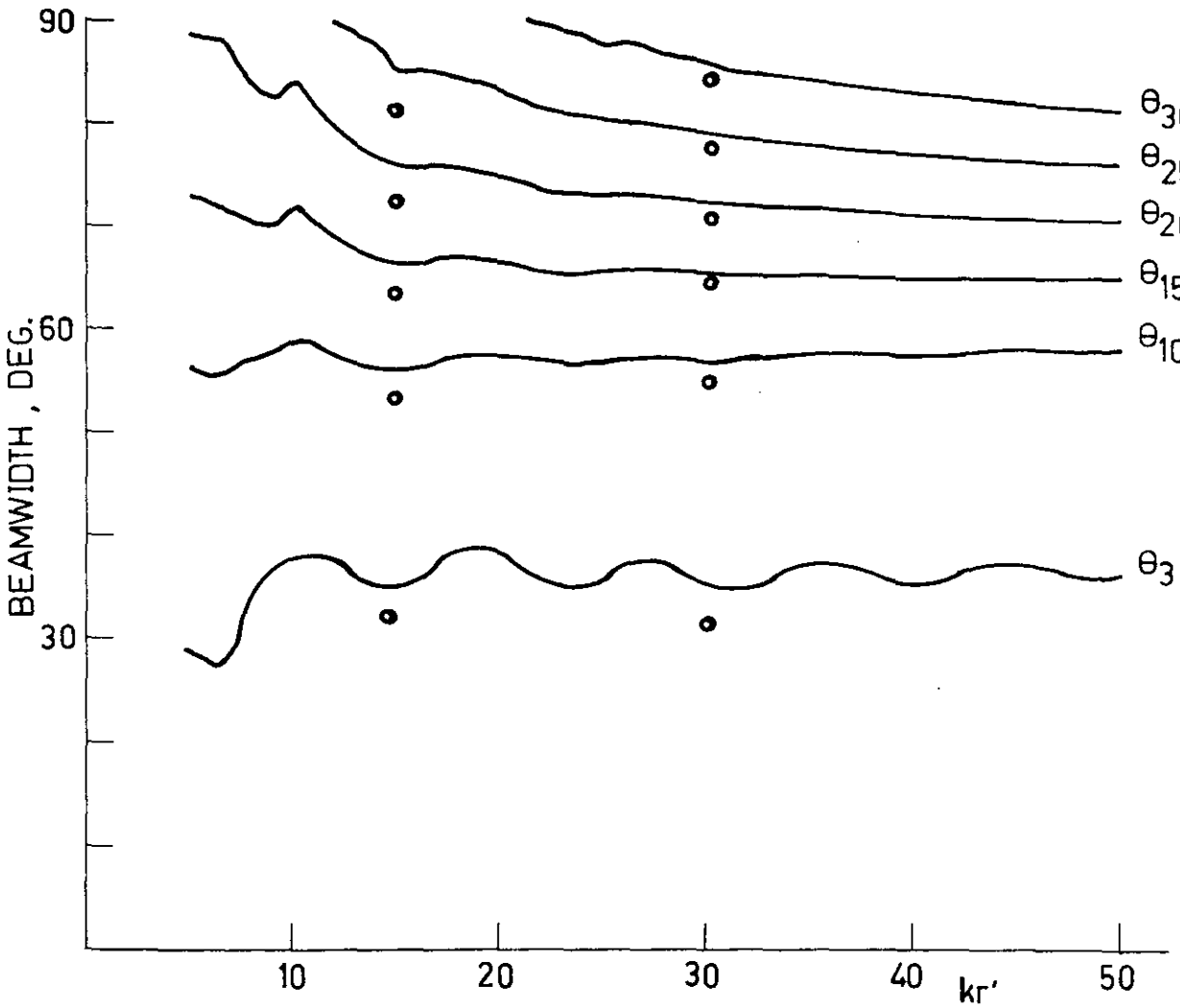

Fig. 15 Beamwidth against kr' for $\theta_o = 75^\circ$; dots indicate experimental results obtained with the antennas 14 and 15 at a frequency of 14 GHz.

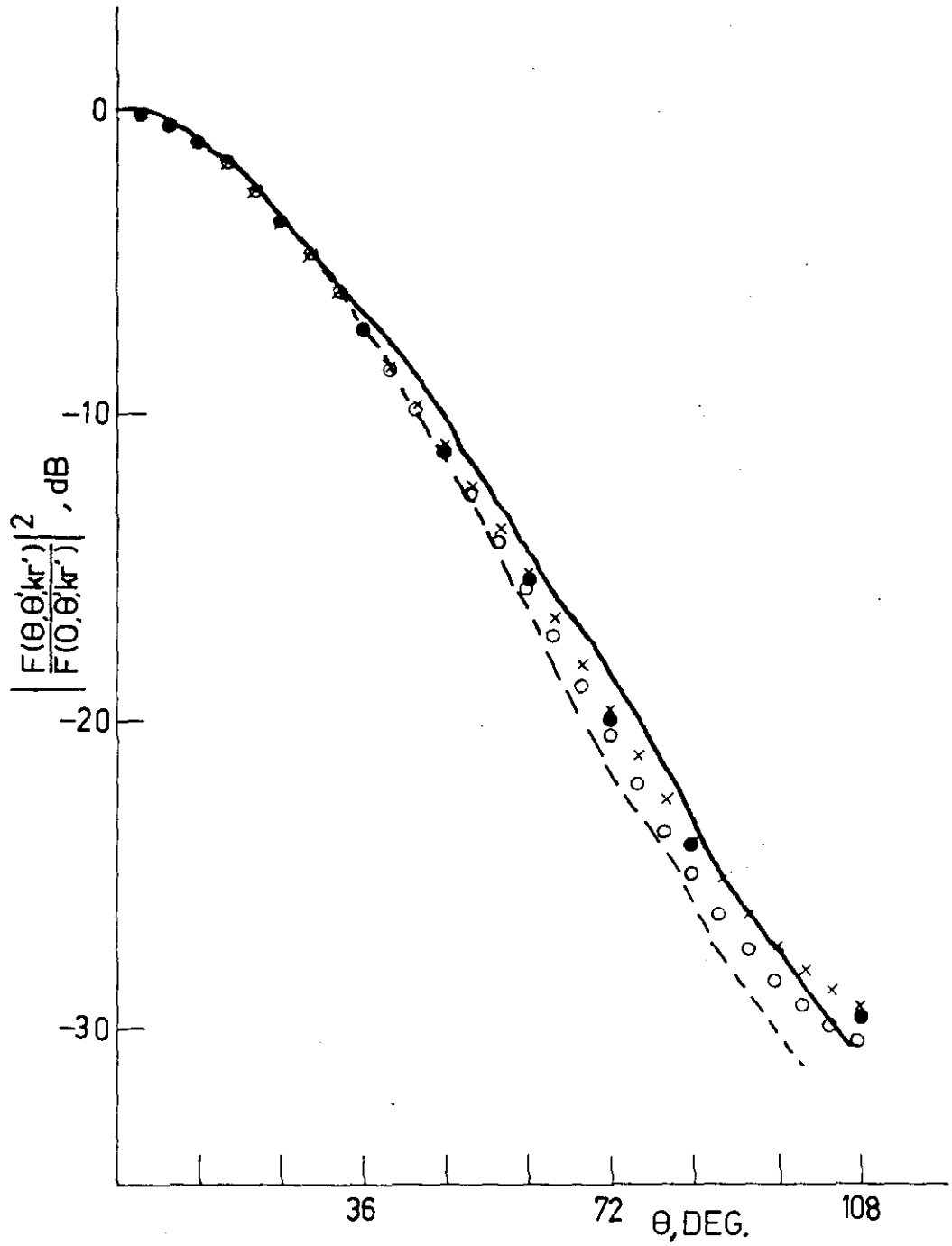

Fig. 16 Radiation pattern of antenna 11.

Calculated ; $\varepsilon_v(kr') = -1$ ● H-plane ; ● E-plane

Calculated ; $\varepsilon_v(kr') \neq -1$ × H-plane ; ○ E-plane

experimental results ; frequency 14 GHz.

———— E-plane

-------- H-plane

It should be noted that the computations from which the Fig.11 to Fig.15 incl. are derived, are based on the assumption that $E_{\phi'} = 0$ and $Z_o H_{\phi'} = 0$ at the boundary $\theta' = \theta_o$. If it is possible to realise the above boundary condition independent of the frequency, then broadband feeds can be realised and Fig.11 to Fig. 15 incl. can be used as design charts. In section 4.2 we shall discuss the practical use of these charts and their limitations.

4.2 Experimental investigation of the corrugated conical horn antenna

4.2.1 $\lambda/4$ - grooves

A comparison of the theory of 4.1 with experimental results is possible, provided the depth of the grooves is a quarter of a wavelength, because only in that case the boundary condition $Z_o H_{\phi'} = 0$ is satisfied. However, there are two exceptions. First, we conclude from Fig.5 that the depth of the grooves should be larger than a quarter of a wavelength if the flare angle Θ_o is small. For the case of a flare angle $\Theta_o = 15^o$ some experimental results have already been published [15]. Secondly, for short horn antennas the boundary condition $E_{\phi'} = 0$ cannot be satisfied with the simple electromagnetic field given in the expressions (39) to (42) incl. However, a useful approximation is discussed in [14], where experimental results are also given. Although the experimental results of [14] and [15] show good agreement with the theoretical predictions, there is a need for a more extensive experimental verification of the theoretical curves of Fig. 11 to Fig. 15 incl. Therefore, several antennas have been constructed in such a way that a wide variation in both the flare angle Θ_o and the length r' of the antennas was obtained. All the grooves were of the same depth and this was a quarter of a wavelength at the frequency 14 GHz.

It should be noted that the antenna with $\Theta_o = 15^o$ is an exception to this rule. The relevant dimensions of the antennas are listed in Table I.

Table I

antenna	θ_o	r' [cm]	d [cm]	b [cm]	t [cm]
1	15°	17.60	0.9	0.20	0.20
2	30°	3.50	0.535	0.26	0.04
3	30°	4.20	0.535	0.26	0.04
4	30°	6.60	0.535	0.26	0.04
5	30°	9.00	0.535	0.26	0.04
6	45°	2.78	0.535	0.26	0.04
7	45°	3.71	0.535	0.26	0.04
8	45°	6.17	0.535	0.26	0.04
9	45°	8.66	0.535	0.26	0.04
10	45°	13.57	0.535	0.26	0.04
11	60°	2.80	0.535	0.26	0.04
12	60°	4.00	0.535	0.26	0.04
13	60°	13.64	0.535	0.26	0.04
14	75°	5.08	0.535	0.26	0.04
15	75°	10.23	0.535	0.26	0.04

The radiation pattern of these antennas has been measured for 14 GHz and the results are plotted in Fig. 11 to Fig. 15 incl. For short antennas the average values of the beamwidths in the H-plane and the E-plane have been plotted. The conclusion is that the experimental results are in good agreement with the theoretical predictions, expecially for $\theta_o \cdot 75^\circ$. If the flare angle $\theta_o = 75$, then there exists a discrepancy between theory and experiment, but the radiation pattern is still symmetrical.

It is very interesting to investigate the effect of the length r' of the antenna on the radiation pattern. For this purpose the radiation patterns of two antennas with the same flare angle but different lengths have been given in Fig. 17. To hold the picture clear we have not plotted the theoretical patterns in Fig. 17, but the agreement is good, especially for the large antenna. We see that a large antenna has a flat radiation pattern and is very suitable as a feed in a paraboloid reflector antenna. It seems that the greatest length that can be used is not determined by electrical requirements but morely by mechanical ones, such as weight and space.

For the application of corrugated conical horn antennas it is necessary that they can be used also for other frequencies than for which the grooves have a depth of a quarter of a wavelength. This question is discussed in section 4.2.2.

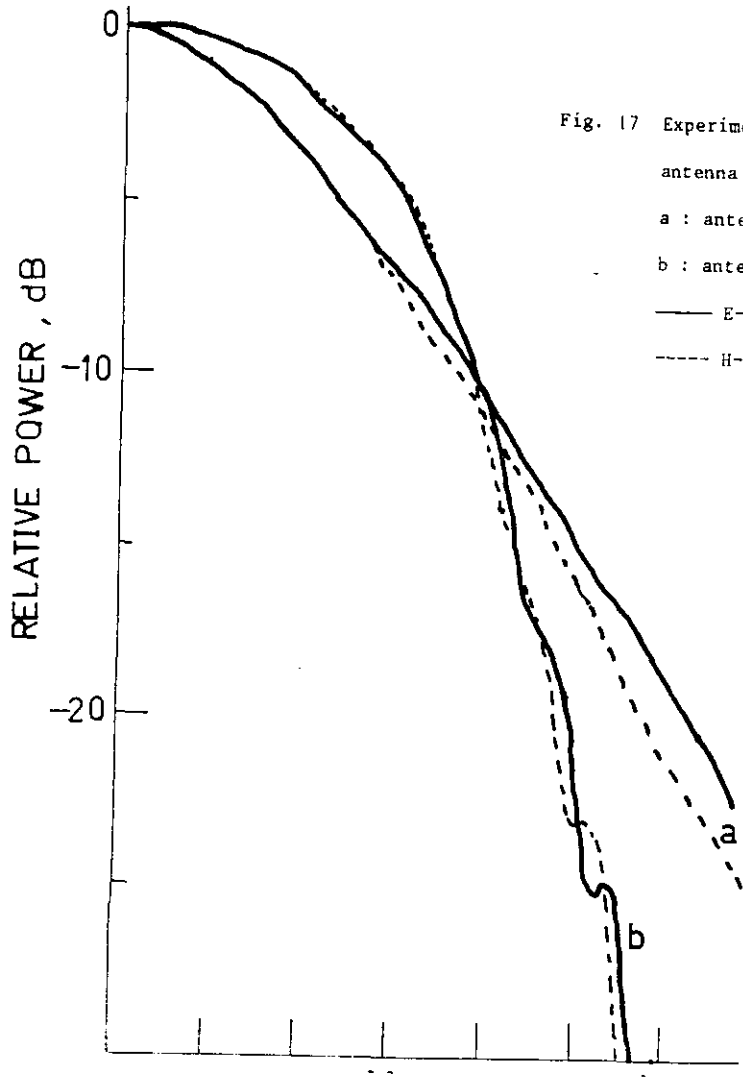

Fig. 17 Experimental radiation pattern of a large antenna and a short antenna with the same flare angle; frequency 14 GHz.
a : antenna 11
b : antenna 13
—— E-plane
----- H-plane

4.2.2 The bandwith of the corrugated conical horn antenna

The bandwidths of the antennas listed in Table I have been studied by measuring the radiation pattern of each of them as a function of the frequency. Lack of space compels us to give only some illustrative examples. Before discussing the experimental results obtained with these antennas we would prefer to summarise first the considerations which have led to the choice of the dimensions of the antennas. From the results of section 4.1 we conclude that good radiation patterns are obtained if we choose kr' large. To obtain the physical dimensions of the antennas within reasonable limits it was decided to carry out the measurements for frequencies higher than 10 GHz.

The diameter of the circular waveguide, which is coupled to the cone, was so chosen that the cut-off frequency of the dominant TE_{11}-mode was approximately 10 GHz. The diameter of the waveguide is 18mm. In Table II we have collected the cut-off frequencies f_c of the higher modes, which will probably be excited at the transition of waveguide to cone if the frequency is raised.

Table II

mode	f_c GHz
TE_{11}	9.767
TM_{01}	12.760
TE_{21}	16.203
TM_{11}	20.332

From this table we see that three higher modes can be excited if the frequency is raised to above 20 GHz. However, the TM_{01} mode and the TE_{21} mode do not have the same φ'-dependence as the TE_{11} mode.

So it is reasonable to assume that these two modes will not be excited. This is not the case for the TM_{11} mode, which has the same ϕ'-dependence as the dominant mode. So it was decided to restrict the measurements to frequencies below 20 GHz. To prevent a large mismatch the lowest frequency was chosen to be 12 GHz. In [16] it is stated that the depth of the grooves should be larger than a quarter of a wavelength in order to prevent the occurence of a surface wave. With a view to investigating this phenomenon we have chosen the depth of the grooves so that at 14 GHz it is a quarter of a wavelength.

For conveniently constructing the antennas the depth of all the grooves was chosen equal and the boundaries of the grooves as straight lines.

The purpose of the measurements which have been carried out can be formulated as follows:

(i) to study surface wave phenomena, if any;

(ii) to prove that a symmetrical radiation pattern is obtained if the depth of the grooves is a quarter of a wavelength. These measurements have already been discussed in the previous section;

(iii) to investigate the deviation between the experimental and the theoretical results of Fig. 11 to Fig. 15 incl., which are based on the assumption that $Z_o H_\phi$, and E_ϕ, are zero, independent of the frequency.

The results of the measurements of the antennas are plotted in Fig. 18 to Fig. 23 incl. The solid line indicates the theoretical beamwidth, based on the assumption that $Z_o H_\phi$, and E_ϕ, are zero. The main conclusion is that the scalar feed is indeed a broadband feed. On closer eximination we observe that for frequencies for which the depth of the grooves is smaller than a quarter of a wavelength, a sudden change occurs in the shape of the radiation pattern.

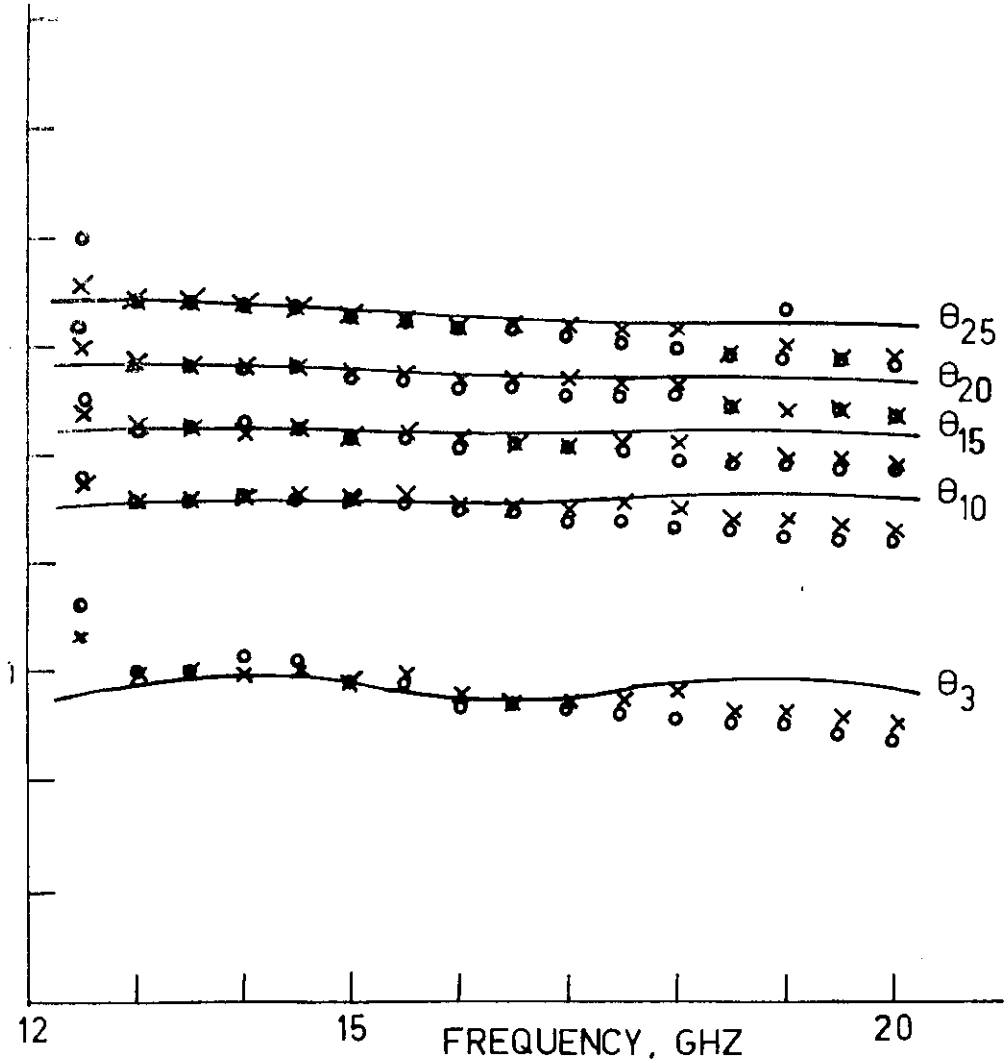

Fig. 18 Beamwidth against frequency; antenna 13;

—— calculated, E-plane and H-plane;

o experiment, E-plane;

× experiment, H-plane;

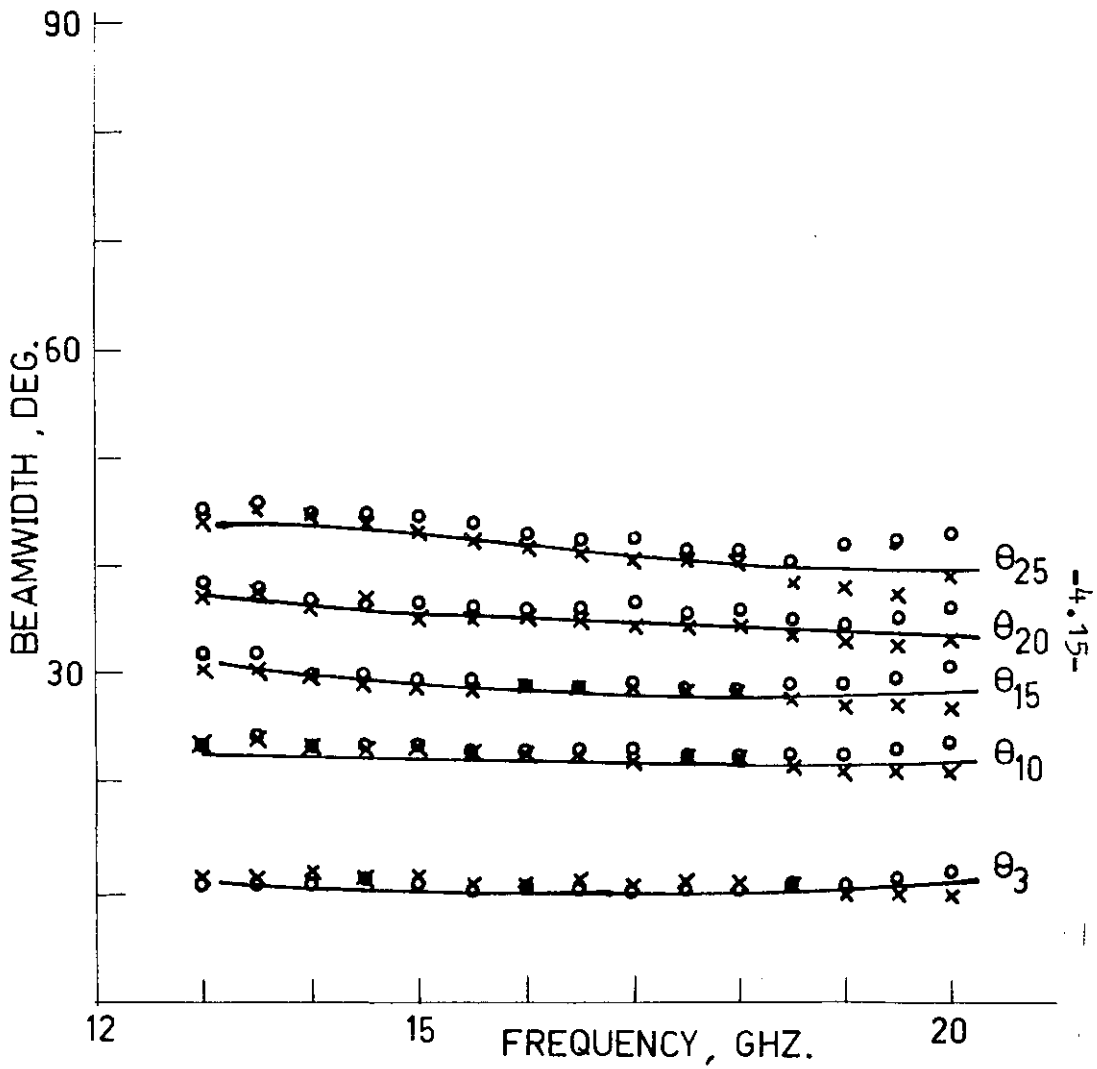

Fig. 19 Beamwidth against frequency; antenna 5 ;

—— calculated, E-plane and H-plane;

o experiment, E-plane;

× experiment, H-plane;

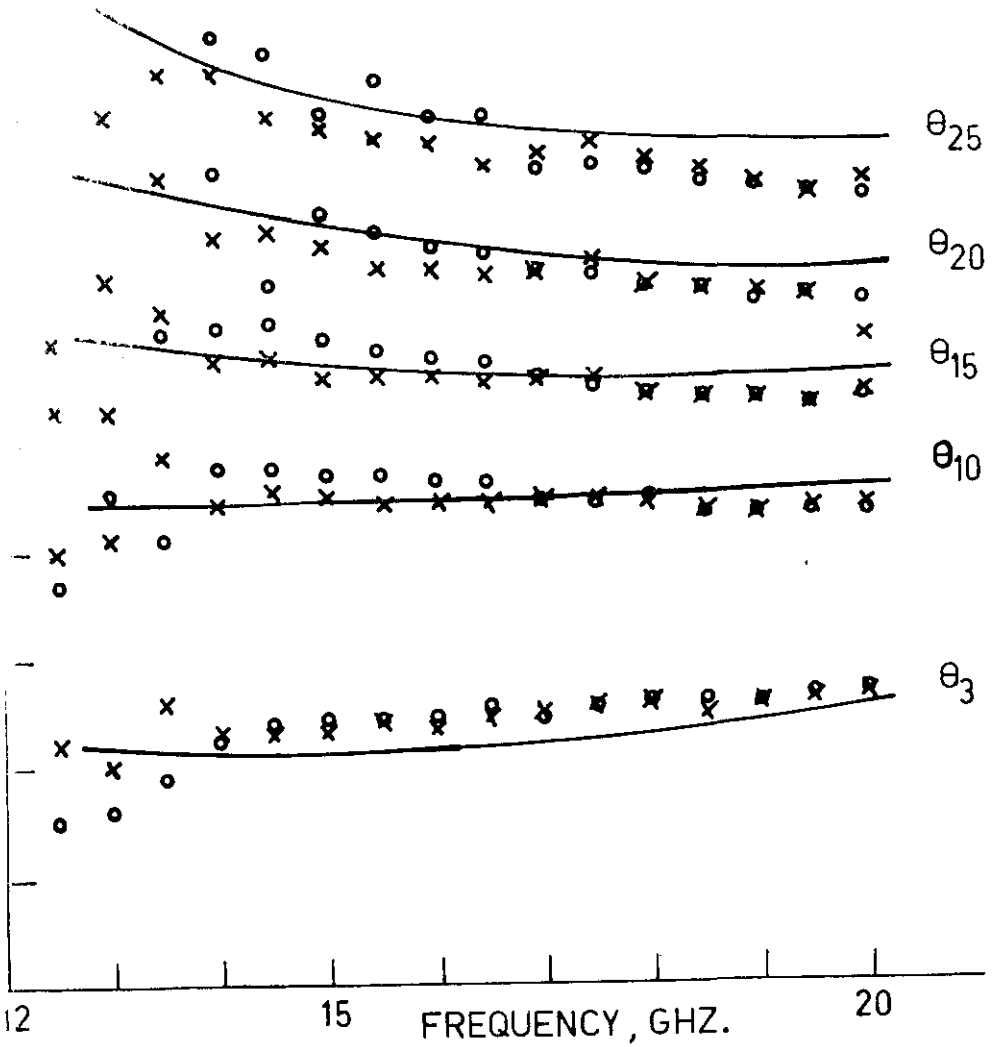

Fig. 20 Beamwidth against frequency; antenna 11;

—— calculated, E-plane and H-plane;

o experiment, E-plane;

× experiment, H-plane;

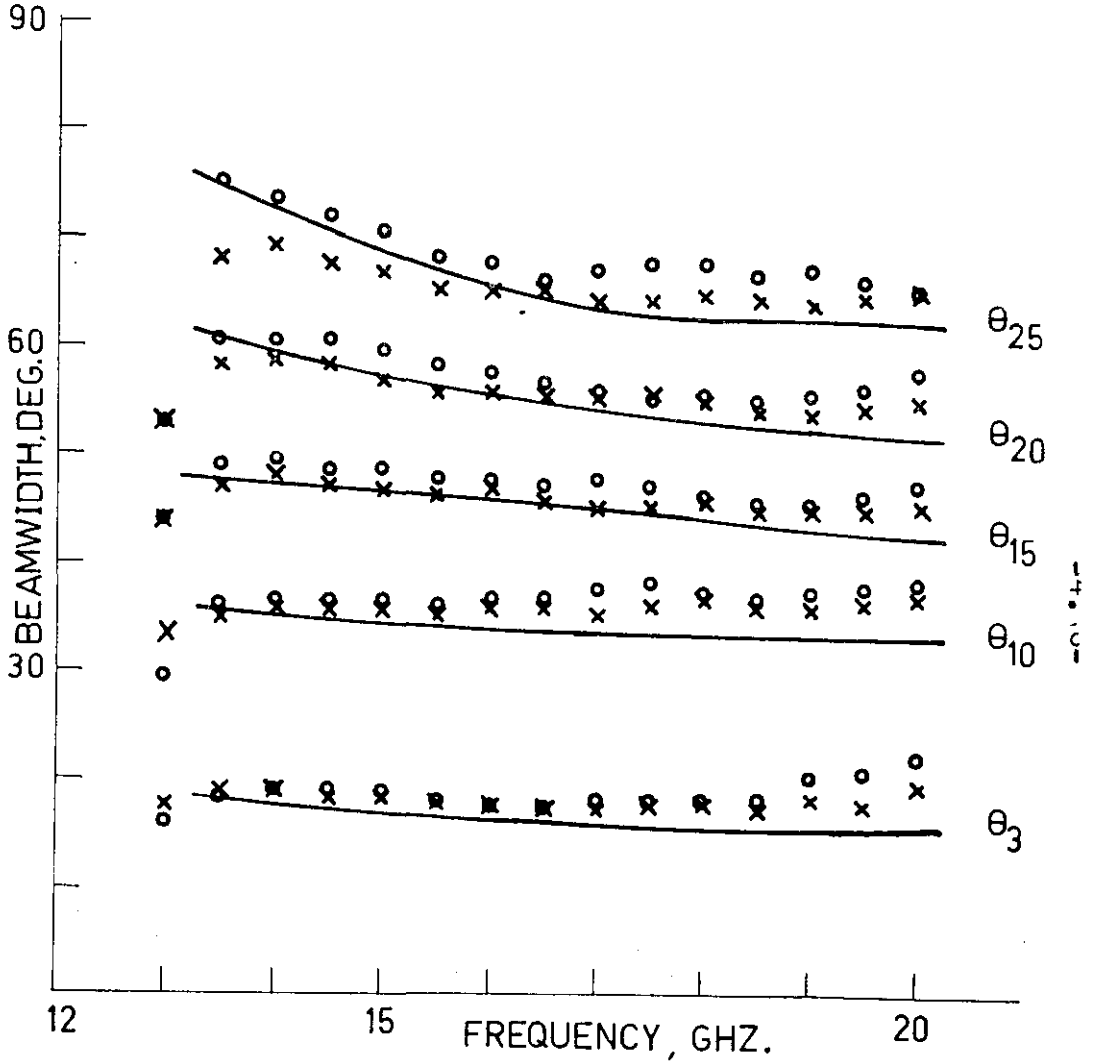

Fig. 21 Beamwidth against frequency; antenna 7;

—— calculated, E-plane and H-plane;

o experiment, E-plane;

× experiment, H-plane;

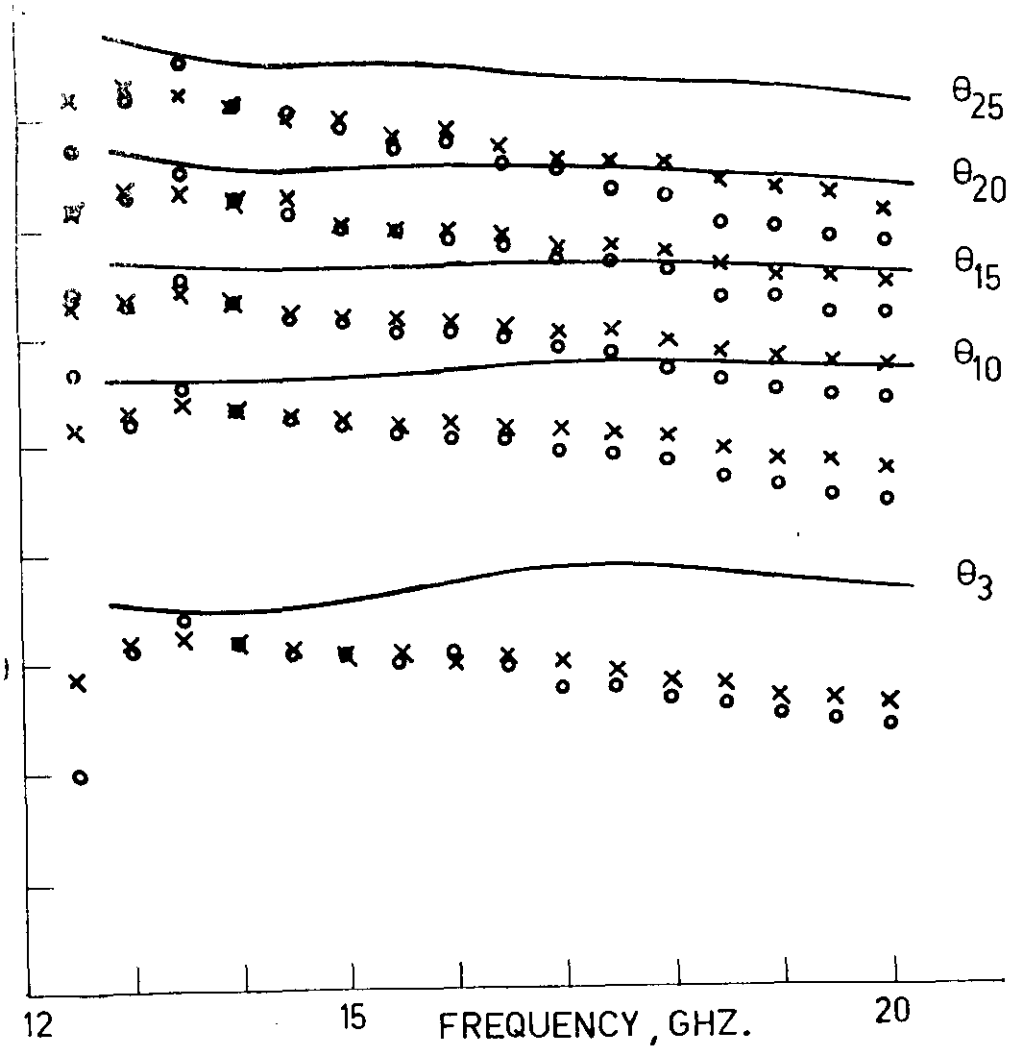

Fig. 22 Beamwidth against frequency; antenna 14;

—— calculated, E-plane and H-plane;

o experiment, E-plane;

× experiment, H-plane;

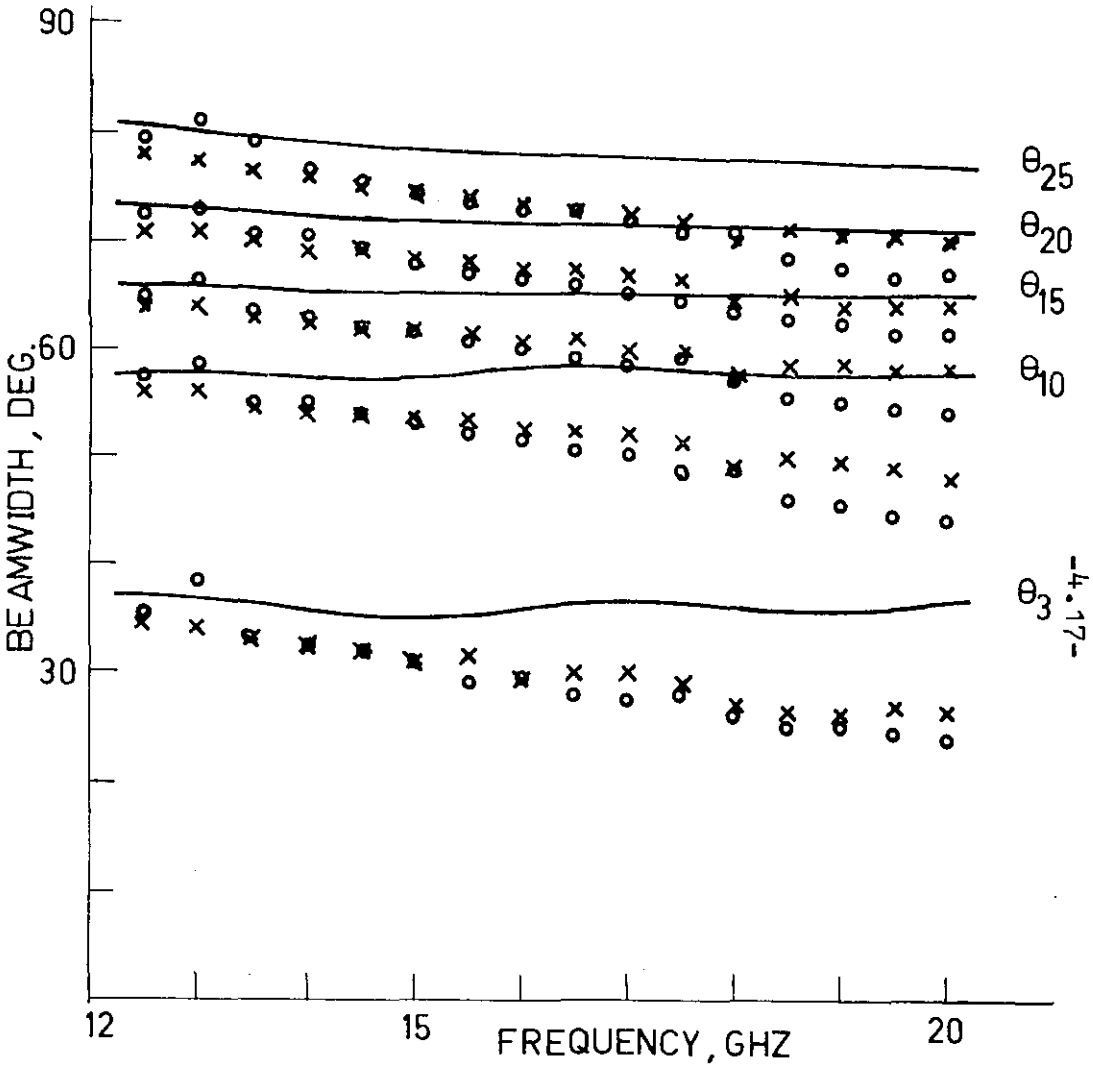

Fig. 23 Beamwidth against frequency; antenna 15;

—— calculated, E-plane and H-plane;

o experiment, E-plane;

× experiment, H-plane;

Probably this is caused by a surface wave, as discussed by Kay [16], and it is claer that for the moment this phenomenon determines the lower limit of the frequency band for which the scalar feed can be used. For frequencies between 14 GHz and 20 GHz we observe a good agreement between the experimental results and the theoretical ones represented by the solid line, provided the flare angle is smaller than 75^{o} and the length of the horns is large. Apparently we may conclude that the boundary conditions $Z_{o}H_{\phi'} = 0$ and $E_{\phi'} = 0$ are valid in a rather large frequency range. This fact gives us the opportunity to use Fig. 11 to Fig. 15 incl. as design charts. We see that if the horns are short and the flare angle is smaller than 75^{o}, the patterns are still symmetrical in the frequency band 14 GHz to 20 GHz, but the agreement between the theory and the experimental results is not so good. In this case Fig. 11 to Fig. 15 incl. can be used only to estimate the beamwidth for frequencies for which the depth of the grooves is not a quarter of a wavelength. From Fig. 22 and Fig. 23 we observe that there is a discrepancy between theory and experiment, if the flare angle $\theta_{o} = 75^{o}$ even if the length of the horn is large.

We see that in this case, too, the radiation pattern is symmetrical. The above discrepancy is probably caused by the excitation of higher spherical hybrid modes.

We also have investigated the V.S.W.R. of the antennas as a function of the frequency. One typical example is given in Fig. 24. Unfortunately, there is a large mismatch at the frequency for which the depth of the grooves is a quarter of a wavelength. However, we have also seen that for frequencies higher than the one mentioned above good radiation patterns are obtained. So it is recommendable to choose the depth of the grooves a little larger than a quarter of a wavelength for the lowest frequency for which the antenna will be used. In that case, a good matching and a good pattern are

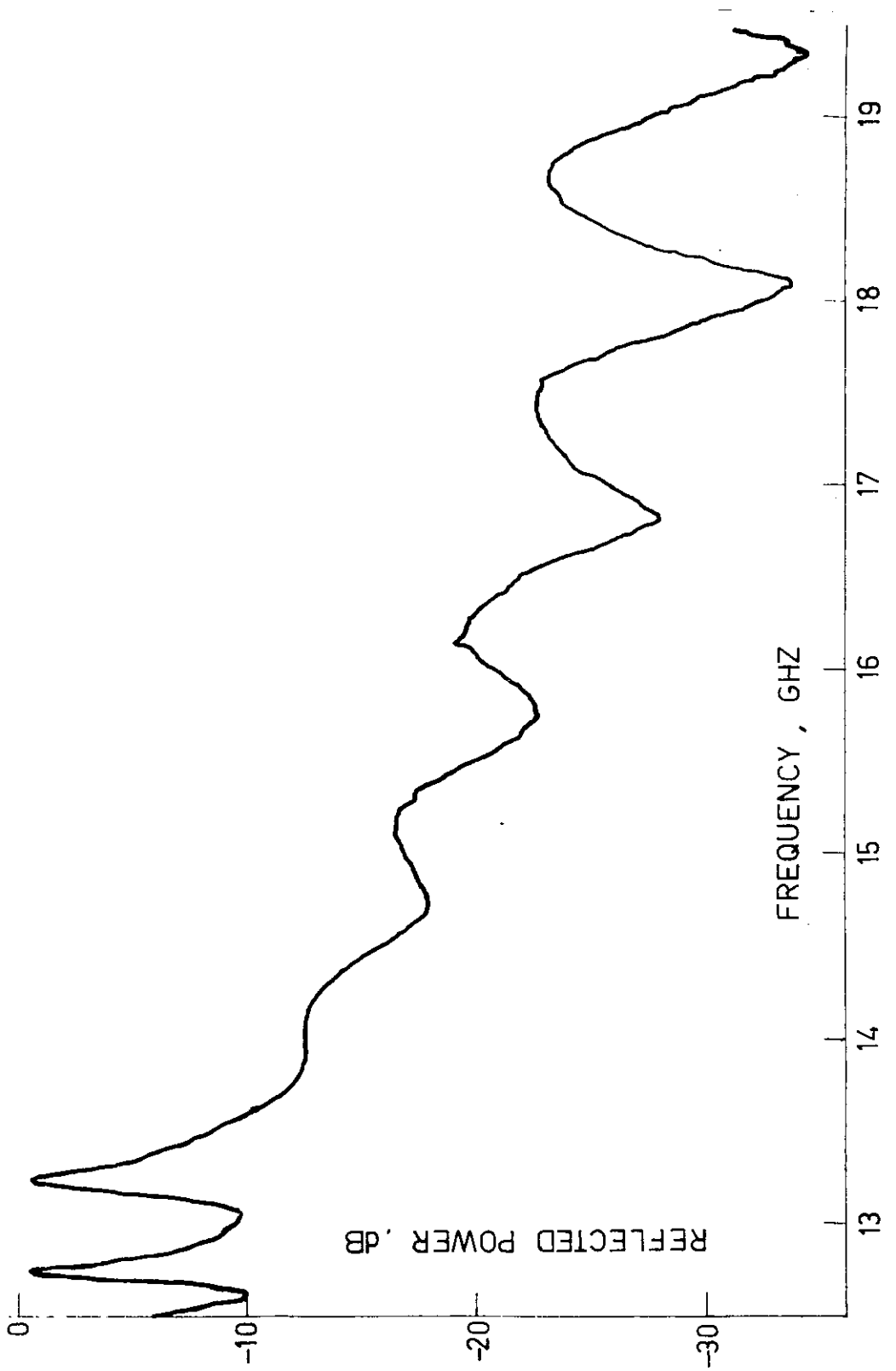

Fig. 2: Measured reflected power against frequency; antenna 7

To study the influence of the thickness of the dams we have investigated the properties of an antenna with the same flare angle and the same length of the horn antenna as antenna 9. The depth of the grooves was also 0.535 cm, but the thickness of the dams was 0.34 cm. After measuring the radiation pattern as a function of the frequency we observed that antenna 9 was better with regard to the bandwidth. Finally, we have constructed two antennas. In the first antenna the depth of the grooves was a quarter of a wavelength at the frequency of 14 GHz. The second antenna has grooves with a depth equal to three quarters of a wavelength at the above frequency. The other dimensions of the two antennas were identical. The antennas exhibited the same radiation pattern at 14 GHz. This is in good agreement with the theoretical prediction (27).

5. Conclusions

The electromagnetic field in the conical corrugated horn antenna and its radiation pattern have been studied theoretically. The main conclusion of this investigation is that the conical corrugated horn antenna has a symmetrical radiation pattern, provided the depth of the grooves is a quarter of a wavelength. The theory of the scalar feed has been formulated for this case. An experimental investigation shows that there is a good agreement between the experimental results and the theoretical calculations if the depth of the grooves is a quarter of a wavelength. Many measurements have been carried out at frequencies of 14 GHz to 20 GHz. From these measurements we can draw the following conclusions. For large antennas with a flare angle θ_o smaller than 75^o there is a good agreement between experimental results and calculations based on the assumption that E_ϕ, and $Z_o H_\phi$, are zero at the boundary $\theta = \theta_o$, even at frequencies for which the depth of the grooves is not equal to a quarter of a wavelength. In case the flare angle is smaller than 75^o and the antennas are short, again resonable agreement between theory and experiment has been found. The measurement of the V.S.W.R. shows that one should choose the depth of the grooves a little larger than a quarter of a wavelength for the lowest frequency for which the antenna will be used. The highest frequency which can be used is determined by the fact that the excitation of higher modes has to be prevented. An improvement of the bandwidth of the waveguide coupled to the cone will probably result in improvement of the bandwidth of the antenna.

Acknowledgements

The authors wish to thank Prof.dr.ir.A.v.Trier for giving them the opportunity to carry out the research described in this report. The discussions with Prof.ir.C.A.Muller concerning the application of the scalar feed in antennas for radio astronomical investigations are greatly appreciated.
Mr.H.Maréchal's and Mr.A.Neyts' skill in accurately constructing the antennas contributed notably to the project. The authors appreciate the assistance of Mr.M.Knoben for the measurements carried out. Finally, they thank Mrs.C.de Haas for devotely typing the paper.

References

1 Simmons A.J. and Kay, A.F.: "The scalar feed - a high performance feed for large paraboloid reflectors", I.E.E. Conference Publication 21, 1966, pp 213 - 217.

2 Jeuken, M.E.J. and Kikkert, J.S.: "A broadband aperture antenna with a narrow beam," Alta Frequenza, vol. XXXVIII, Maggio 1969, Numero Speciale, pp 270 - 276.

3 Harrington, R.F.: "Time-harmonic electromagnetic fields", Chapter 6, Mc Graw-Hill 1961.

4 Abramowitz, M. and Stegun, I.A.: "Handbook of Mathematical Functions", p 437, Dover Publication, New York.

5 Abramowitz, ibid, p 439.

6 Abramowitz, ibid, p 336.

7 Harrington, ibid, p 469.

8 Dixon, G., Jarvis, T.R. and White, I.: "Angular-dependent modes in circular corrugated waveguide." Proc. I.E.E. vol.110, no.8, August 1963.

9 Modern Computing Methods, National Physical Laboratory London, Notes on Applied Science, no. 16, Her Majesty's Stationery Office 1961.

10 Wilkinson, J.H.: "Calculation of the eigenvalues of a symmetric tridiagonal matrix by the method of bisection" Numerische Mathematik,4, S 362 - 367.

11 Gray, W.: "On extrapolation algorithms for ordinary initial value problems." Journal Siam Numerical Analysis, B 2, pp 384 - 403

12 Zonneveld, J.A.: "Automatic Numerical Integration", Mathematisch Centrum Amsterdam, 1964.

13. Flügge, S.: "Handbuch der Physik", Bd 25, S 238 - 240 Springer-Verlag, Berlin, Göttingen, Heidelberg, 1961.

14 Jeuken, M.E.J. and Lambrechtse, C.W.: "Small corrugated conical horn antenna with wide flare angle", Electronics Letters, 1969, 5, pp 489-490.

15 Jeuken, M.E.J.: "Experimental radiation pattern of the corrugated conical horn antenna with small flare angle", Electronics Letters, 1969, 5, pp 484 - 485.

16 Kay, A.F.: "The scalar feed", TRG report, contract AF 19(604) - 8057, March 1964.

Appendix A

In this appendix we shall describe a method of finding the solution of (4). This means to find n for prescribed kr_1 and kr_2. The problem is equivalent to the problem of finding the value of n in the Bessel equation

$$\frac{d}{dr}\left(r^2 \frac{dR}{dr}\right) + \left\{(kr)^2 - n(n+1)\right\} R = 0 \qquad (A.1)$$

subjected to the boundary conditions $R(r) = 0$ for $r = r_1$ and $r = r_2$.

Let us use the abbreviations $x = kr$, $kr_1 = a$, $kr_2 = b$ and $n(n+1) = \lambda$.

Next we shall transform equation (A.1) to a set of difference equations. The difference approximation of $\frac{d}{dx}\left(x^2 \frac{dR}{dx}\right)$ is given by [9]:

$$\frac{x_{j+\frac{1}{2}}^2 (R_{j+1} - R_j) - x_{j-\frac{1}{2}}^2 (R_j - R_{j-1})}{\Delta^2} + O(\Delta^2) \qquad (A.2)$$

with $R_j = R(x_j)$, $x_j = a + j\Delta$ and $\Delta = (b-a)(M+1)$.

(See Fig. A.1)

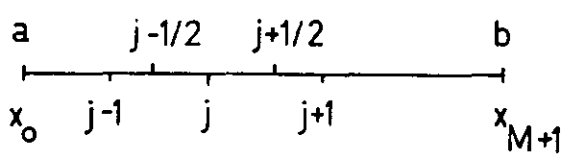

Fig.A1

Substitution of (A.2) in (A.1) gives

$$\left(\frac{x_{j-\frac{1}{2}}}{\Lambda}\right)^2 R_{j-1} + \left[-\left(\frac{x_{j+\frac{1}{2}}}{\Lambda}\right)^2 - \left(\frac{x_{j-\frac{1}{2}}}{\Lambda}\right)^2 + x_j^2\right] R_j + \left(\frac{x_{j+\frac{1}{2}}}{\Lambda}\right)^2 R_{j+1} = \lambda R_j \quad (A.3)$$

Applying the boundary conditions $R_o = R_{M+1} = 0$ by substitution of $j = 1$ and $j = M$ respectively in (A.3) gives rise to the next two equations

$$\left[-\left(\frac{x_{3/2}}{\Lambda}\right)^2 - \left(\frac{x_{\frac{1}{2}}}{\Lambda}\right)^2 + x_1^2\right] R_1 + \left(\frac{x_{3/2}}{\Lambda}\right)^2 R_2 = \lambda R_1 \quad (A.4)$$

and

$$\left(\frac{x_{M-\frac{1}{2}}}{\Lambda}\right)^2 R_{M-1} + \left[-\left(\frac{x_{M+\frac{1}{2}}}{\Lambda}\right)^2 - \left(\frac{x_{M-\frac{1}{2}}}{\Lambda}\right)^2 + x_M^2\right] R_M = \lambda R_M \quad (A.5)$$

Equations (A.3), (A.4) and (A.5) together can be written as an problem of a symmetrical tridiagonal matrix

$$\begin{pmatrix} \times & \times & & & \\ \times & \times & \times & & \\ & \ddots & \ddots & \ddots & \\ & & \times & \times & \times \\ & & & \times & \times \end{pmatrix} \begin{pmatrix} R_1 \\ R_2 \\ \vdots \\ R_{M-1} \\ R_M \end{pmatrix} = \lambda \begin{pmatrix} R_1 \\ R_2 \\ \vdots \\ R_{M-1} \\ R_M \end{pmatrix} \quad (A.6)$$

Equation (A.6) has been used for the computation of λ and thus of n as a function of kr_1 and kb [9], [10]. The results are collected in Fig.3. It shouls be noted that the value n is associated with the dominant mode.

Appendix B

To find the value of n which satisfied (12) we adopt the same procedure as used in appendix A. Now we have to solve (A.1), but with the boundary conditions

$$\frac{d}{dr}(rR) = 0 \quad \text{for } r = r_1 \text{ and } r = r_2 \tag{B.1}$$

In this case we find again

$$\left(\frac{x_{j-\frac{1}{2}}}{\Delta}\right)^2 R_{j-1} + \left[-\left(\frac{x_{j+\frac{1}{2}}}{\Delta}\right)^2 - \left(\frac{x_{j-\frac{1}{2}}}{\Delta}\right)^2 + x_j^2\right] R_j + \left(\frac{x_{j+\frac{1}{2}}}{\Delta}\right)^2 R_{j+1} = \lambda R_j \tag{B.2}$$

A difference approximation of the boundary conditions (B.1) yields

$$x_1 R_1 - x_{-1} R_{-1} = 0 \tag{B.3}$$

and

$$x_{M+2} R_{M+2} - x_M R_M = 0 \tag{B.4}$$

Substitution of $j = 0$ in (B.2) and application of the condition (B.3) gives

$$\left[-\left(\frac{x_{\frac{1}{2}}}{\Delta}\right)^2 - \left(\frac{x_{-\frac{1}{2}}}{\Delta}\right)^2 + x_0^2\right] R_0 + \left[\left(\frac{x_{-\frac{1}{2}}}{\Delta}\right)^2 \frac{x_1}{x_{-1}} + \left(\frac{x_{\frac{1}{2}}}{\Delta}\right)^2\right] R_1 = \lambda R_0 \tag{B.5}$$

Substitution of $j = M+1$ in (B.2) and application of the condition (B.4) gives

$$\left[\left(\frac{x_{M+\frac{1}{2}}}{\Delta}\right)^2 + \left(\frac{x_{M+3/2}}{\Delta}\right)^2 \frac{x_M}{x_{M+2}}\right] R_M + \left[-\left(\frac{x_{M+3/2}}{\Delta}\right)^2 - \left(\frac{x_{M+\frac{1}{2}}}{\Delta}\right)^2 + x_{M+1}^2\right] R_{M+1} = \lambda R_{M+1} \tag{B.6}$$

Unfortunately, it is not possible to take the equations (B.2), (B.5) and (B.6) together and to write them as an eigenvalue problem of a symmetrical tridiagonal matrix with the same eigenvalues which are of interest to us, but with slightly different eigenvectors. After some algebraical manupulations we find the matrix mentioned above, provided we substitute

$$\alpha_o R_o = R^*_o$$

$$\text{with} \quad \alpha_o = \frac{x_{\frac{1}{2}}}{\Lambda}\left[\left(\frac{x_{\frac{1}{2}}}{\Lambda}\right)^2 + \left(\frac{x_{-\frac{1}{2}}}{\Lambda}\right)^2 \frac{x_1}{x_{-1}}\right]^{\frac{1}{2}} \tag{B.7}$$

$$\text{and} \quad \alpha_{M+1} R_{M+1} = R^*_{M+1}$$

$$\text{with} \quad \alpha_{M+1} = \frac{x_{M+\frac{1}{2}}}{\Lambda}\left[\left(\frac{x_{M+\frac{1}{2}}}{\Lambda}\right)^2 + \left(\frac{x_{M+3/2}}{\Lambda}\right)^2 \frac{x_M}{x_{M+2}}\right]^{\frac{1}{2}} \tag{B.8}$$

$$\text{and} \quad \alpha_j R_j = R_j$$

$$\text{with} \quad \alpha_j = 1 \quad \text{for } j = 1, 2 \ldots M. \tag{B.9}$$

After these preparations we find the eigenvalues Λ and thus n from the equation

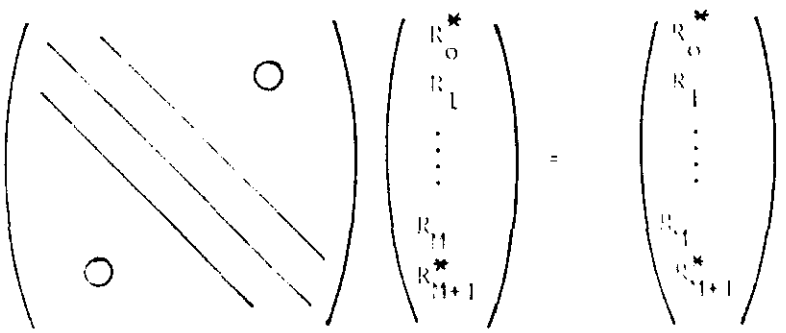

(B.10)

Appendix C

The depth of the groove under the condition that $Z_o H_\phi = 0$ at the opening of the groove can be computed by means of equation (20). However, to find the angle $\theta_1 = \theta_2 - \theta_o$ we do not use (20), but prefer another numerical technique. We have to solve the differential equation of Legendre

$$\frac{1}{\sin\theta}\frac{d}{d\theta}\left(\sin\theta\,\frac{dy(\theta)}{d\theta}\right) + \left[n(n+1) - \frac{1}{\sin^2\theta}\right] y(\theta) = 0 \qquad (C.1)$$

with, for a TM-mode, the homogeneous boundary conditions

$$y'(\cos\theta_o) = 0 \qquad (C.2)$$

and

$$y(\cos\theta_2) = 0 \qquad (C.3)$$

Integrating (C.1) by means of the Runga-Kutta method of second order [12] with initial values

$$y'(\cos\theta_o) = 0 \qquad (C.2)$$

and

$$y(\cos\theta_o) = 1 \qquad (C.4)$$

until $y(\cos\theta) = 0$, we find the value of θ_2 and thus of $\theta_2 - \theta_o$. It should be noted that the choice $y(\cos\theta_o) = 1$ is permissible because both equations (C.1) and the boundary conditions (C.2) and (C.3) are homogeneous. The results of the computations can be found in Fig. 5.